**This is the accepted manuscript (postprint) of the following article:**
F. Ghanbari, A.H. Taghvaei, E. Salahinejad, M. Pahlevani, Z. Khosrowpour, S.M.A. Haramshahi, M. Gholipourmalekabadi, *Strontium-doped mesoporous bioactive glass reinforced silk fibroin/decellularized extracellular matrix nanocomposite scaffolds for potential bone tissue engineering*, Ceramics International, 51 (2025) 60419-60433.
https://doi.org/10.1016/j.ceramint.2025.10.242

# Strontium-doped mesoporous bioactive glass reinforced silk fibroin/decellularized extracellular matrix nanocomposite scaffolds for potential bone tissue engineering

Farid Ghanbari [a], Amir Hossein Taghvaei [a,b,*], Erfan Salahinejad [c], Majid Pahlevani [b], Zahra Khosrowpour [d], Seyed Mohammad Amin Haramshahi [e,f], Mazaher Gholipourmalekabadi [f,g,h,*]

[a] *Department of Materials Science and Engineering, Shiraz University of Technology, Shiraz, Iran*

[b] *Department of Electrical and Computer Engineering, Queen's University, Kingston, ON, Canada*

[c] *Faculty of Materials Science and Engineering, K. N. Toosi University of Technology, Tehran, Iran*

[d] *Department of Pediatrics, University of Minnesota, Minneapolis, USA*

[e] *Cellular and Molecular Research Center, Iran University of Medical Sciences, Tehran, Iran*

[f] *Department of Tissue Engineering & Regenerative Medicine, Faculty of Advanced Technologies in Medicine, Iran University of Medical Sciences, Tehran, Iran*

[g] *Stem cell and Regenerative Medicine Research Center, Iran University of Medical Sciences, Tehran, Iran*

[h] *Department of Medical Biotechnology, Faculty of Allied Medicine, Iran University of Medical Sciences, Tehran, Iran*

## Abstract

Effective bone tissue engineering requires scaffolds to have both bioactive and mechanical properties to aid in the regeneration of the biochemical and mineral components of bone. In this paper, ternary nanocomposite scaffolds are introduced for the first time, which consist of

* Corresponding authors: A.H.T.: <amirtaghvaei@gmail.com, taghvaei@sutech.ac.ir, NV26@queensu.ca>; M.G.: <mazaher.gholipour@gmail.com>

**This is the accepted manuscript (postprint) of the following article:**
F. Ghanbari, A.H. Taghvaei, E. Salahinejad, M. Pahlevani, Z. Khosrowpour, S.M.A. Haramshahi, M. Gholipourmalekabadi, *Strontium-doped mesoporous bioactive glass reinforced silk fibroin/decellularized extracellular matrix nanocomposite scaffolds for potential bone tissue engineering*, Ceramics International, 51 (2025) 60419-60433.
https://doi.org/10.1016/j.ceramint.2025.10.242

a silk fibroin (SF) matrix reinforced with placenta-derived decellularized extracellular matrix (DCECM) and strontium-containing mesoporous bioactive glass nanospheres (SrMBNs). This composite design aims to overcome the limitations of each individual component and their binary combinations in bone tissue regeneration. For this purpose, the effects of varying the SF:DCECM:SrMBN ratio on the structure, mechanical, degradation, swelling, apatite-forming, cytocompatibility, and pro-osteogenic potential of the scaffolds are systematically investigated. According to results, introducing 30 wt% DCECM transformed the lamellar structure of pure SF into a highly porous architecture of 90% porosity, with enhancements in compressive strength by 170%, swelling ratio by 70%, and *in-vitro* degradation rate by 185%. The incorporation of 15 wt% SrMBNs showed the most satisfactory results in terms of apatite formation, while the degradation and swelling rates of the SF-DCECM scaffolds were minimally affected. The scaffolds with 30% DCECM and 15% SrMBNs exhibited significantly improved attachment, viability, and proliferation of rat bone marrow mesenchymal stem cells (rBMSCs) compared to the pure SF scaffolds. Alizarin Red S staining confirmed that with the SrMBNs, there was greater calcium deposition, indicative of more osteogenic potential in comparison to the SF/DCECM scaffolds. Collectively, the SF/DCECM/SrMBNs scaffolds exhibited superior physicochemical, mechanical, and biological performances, with strong potential as bone-mimetic platforms for bone regeneration applications.

***Keywords*:** Silk fibroin (SF); Decellularized extracellular matrix; Bioactive glass; Mesoporous nanoparticles

**This is the accepted manuscript (postprint) of the following article:**
F. Ghanbari, A.H. Taghvaei, E. Salahinejad, M. Pahlevani, Z. Khosrowpour, S.M.A. Haramshahi, M. Gholipourmalekabadi, *Strontium-doped mesoporous bioactive glass reinforced silk fibroin/decellularized extracellular matrix nanocomposite scaffolds for potential bone tissue engineering*, Ceramics International, 51 (2025) 60419-60433.
https://doi.org/10.1016/j.ceramint.2025.10.242

## 1- Introduction

Bone is responsible for supporting the body's structure and motion, controlling the pH of blood, maintaining calcium phosphate levels to facilitate important physiological functions, and protecting vital organs such as the brain and bone marrow [1, 2]. Nevertheless, critical-sized defects in bone are a significant clinical problem since such defects do not close spontaneously without some form of medical intervention. To treat this condition, clinical practice extensively utilizes autografts, allografts, and xenografts. Despite their effectiveness, each of these approaches exhibits important disadvantages, such as additional tissue harvesting required in autografts, donor site morbidity, risk of infection transmission, immunological rejection, and restricted availability of donors [3, 4]. Alternatively, tissue engineering has appeared as a hopeful path to fix bone defects or dysfunctions and enhance bone recovery. It is widely accepted that artificial bone scaffolds must mimic the structure and functional properties of healthy bone to be effective in bone regeneration applications. Besides, they must have biocompatibility, asset cell attachment, and promote cell growth and differentiation to facilitate bone tissue regeneration [4, 5].

Silk fibroin (SF), derived from *Bombyx mori*, is a well-known sericulture product that has a simple manufacturing process and exhibits a desired physiochemical behavior (e.g., decent biocompatibility and bioresorbability), a low immunity response, and adjustable biomechanical properties [6, 7]. Biomaterials based on SF can be made into varying shapes like films, hydrogels, sponges, 3D forms, and nanoparticles. They have obtained the US Food and Drug Administration (FDA) approval for usage in sutures, and many investigators have been interested in them due to their prospect of making scaffolds for various kinds of tissue

**This is the accepted manuscript (postprint) of the following article:**
F. Ghanbari, A.H. Taghvaei, E. Salahinejad, M. Pahlevani, Z. Khosrowpour, S.M.A. Haramshahi, M. Gholipourmalekabadi, *Strontium-doped mesoporous bioactive glass reinforced silk fibroin/decellularized extracellular matrix nanocomposite scaffolds for potential bone tissue engineering*, Ceramics International, 51 (2025) 60419-60433.
https://doi.org/10.1016/j.ceramint.2025.10.242

engineering applications, such as bone, cartilage, ligament, tendon, skin, and wound healing for last 20 years. Despite its attractive qualities, SF is typically blended with other materials to improve biocompatibility and osteogenic performance [8-11].

When a bone fractures, proper healing requires an adequate blood supply and the presence of suitable growth factors in the fracture site. As a result, using a scaffold that contains an extracellular matrix (ECM) in the fracture area would be reasonable to deliver growth factors from the outside or trap them from the inside [12]. For this purpose, a decellularized extracellular matrix (DCECM) can demonstrate physical and chemical signals, enhancing the cytocompatibility, proliferation, and differentiation of progenitor/stem cells [13]. Furthermore, DCECM products retain the basic shape, features, biomechanical, and biological activity of the native ECM. The human placenta is one of the most available sources of ECM, and some of its products have been employed in tissue engineering. This is due to the presence of growth factors and cytokines like transforming growth factor-ß (TGF-ß), bone morphogenetic proteins (BMPs), and vascular endothelial growth factor (VEGF) [14]. In addition, the placenta-derived ECM collagen types I, III, IV, V, VI, fibronectin, and laminin—which all play important roles in improved tissue regeneration [15]. In addition, it is typically thrown away and can be collected without compromising the donor's health.

Bioactivity reflects a biomaterial's ability to form a chemical bond with its surrounding tissue by developing a hydroxyapatite (HAp) layer on its surface. This layer mimics the mineral structure of natural bone and enhances chemical bonding between the scaffold and surrounding tissue. In addition, it plays an important role in cellular activities such as osteoblast adhesion, proliferation, and differentiation [16]. Among different bioactive materials, mesoporous bioactive glasses (MBGs) are distinguished for their higher bioactivity compared to

**This is the accepted manuscript (postprint) of the following article:**
F. Ghanbari, A.H. Taghvaei, E. Salahinejad, M. Pahlevani, Z. Khosrowpour, S.M.A. Haramshahi, M. Gholipourmalekabadi, *Strontium-doped mesoporous bioactive glass reinforced silk fibroin/decellularized extracellular matrix nanocomposite scaffolds for potential bone tissue engineering*, Ceramics International, 51 (2025) 60419-60433.
https://doi.org/10.1016/j.ceramint.2025.10.242

conventional bioactive glass (BG). MBGs exhibit an ordered or disordered network of mesopores, typically 2–20 nm in diameter, which can be used to deliver therapeutic ions, drugs, or growth factors. In addition to their high surface area, MBGs degrade more efficiently, releasing osteogenic ions like silicon, calcium, phosphorus, and sodium. These ions could play a crucial role in stimulating both intracellular and extracellular responses, and enhancing cell proliferation and differentiation [17]. However, MBGs are biomechanically weak and degrade rapidly with an unstable surface/interface that could adversely affects cell growth [18, 19]. To overcome this, MBGs can be mixed with biopolymers to interact physically or chemically with their networks and improve their stability. These suggest that MBGs, especially in the form of nanoparticles, are promising filler materials in DCECM-based scaffolds to enhance their physiochemical properties as well as mechanical/chemical stability. Additionally, advantageous biological effects are expected, including cell proliferation, osteogenesis of stem cells, and mineralization. In our previous research [20], we successfully synthesized novel strontium-substituted mesoporous bioactive glass nanospheres (SrMBNs) characterized by spherical morphology, excellent dispersion, and favorable texture properties. Our findings revealed that the synthesized SrMBNs exhibited not only high bioactivity, but also significantly enhanced stem cells proliferation compared to strontium-free samples. This indicates the potential of their dissolution products to promote cellular proliferation and differentiation.

Previous research has highlighted the potential of SF-MBGs scaffolds as superior platforms for bone regeneration, particularly in comparison to SF alone, in terms of bioactivity and physicochemical properties [21, 22]. However, most studies have focused on using micron-sized MBG reinforcements, which may lead to sedimentation during fabrication and an uneven distribution, as well as a lack of replicating the natural ECM of bone which contains nano-

**This is the accepted manuscript (postprint) of the following article:**
F. Ghanbari, A.H. Taghvaei, E. Salahinejad, M. Pahlevani, Z. Khosrowpour, S.M.A. Haramshahi, M. Gholipourmalekabadi, *Strontium-doped mesoporous bioactive glass reinforced silk fibroin/decellularized extracellular matrix nanocomposite scaffolds for potential bone tissue engineering*, Ceramics International, 51 (2025) 60419-60433.
https://doi.org/10.1016/j.ceramint.2025.10.242

apatite crystals. Additionally, SF/MBGs scaffolds cannot fully address the inherent challenges of SF in terms of its unmodified degradation rate and the lack of cell attachment motifs. Although DCECM offers unique advantages, such as the presence of endogenous chemical signals and a structure that closely mimics the biological and mechanical properties of natural ECM, the effectiveness of SF/DCECM scaffolds for bone regeneration remains underexplored. For instance, Sangkert *et al*. [23] combined dental pulp-derived DCECM with fibronectin on SF scaffolds, demonstrating enhanced cellular activity and osteogenic potential for addressing maxillofacial bone defects. Similarly, Rameshbabu *et al*. [14] developed 3D porous SF/placenta-derived DCECM scaffolds via freeze-drying, highlighting their promising capacity for angiogenesis and accelerated bone regeneration compared to SF alone. However, the systematic investigation of how the placenta-derived ECM content influences the structure, physicochemical, mechanical, and osteogenic properties of SF/placenta-derived ECM scaffolds is still lacking. Moreover, none of the existing SF/placenta-derived ECM scaffolds have been optimized for advanced bone regeneration. This originates from the absence of bioceramic fillers, which are important for improving mechanical strength, bioactivity, and osteoinductivity.

Given the limitations of both SF/MBGs and SF/ECM composites, this study focuses on the development of novel SF-based scaffolds reinforced with placenta-derived DCECM and SrMBNs for enhanced bioperformance. The hypothesis behind combining placenta-derived DCECM with SrMBNs is to create a bone-mimicking microenvironment that not only improves the structural, mechanical, and physicochemical properties but also synergistically enhances the cytocompatibility, bioactivity, and osteogenic potential of SF. To the authors'

**This is the accepted manuscript (postprint) of the following article:**
F. Ghanbari, A.H. Taghvaei, E. Salahinejad, M. Pahlevani, Z. Khosrowpour, S.M.A. Haramshahi, M. Gholipourmalekabadi, *Strontium-doped mesoporous bioactive glass reinforced silk fibroin/decellularized extracellular matrix nanocomposite scaffolds for potential bone tissue engineering*, Ceramics International, 51 (2025) 60419-60433.
https://doi.org/10.1016/j.ceramint.2025.10.242

knowledge, this is the first research focused on developing this ternary composite scaffold for advanced bone reconstruction applications.

## 2- Materials and methods

### 2-1- Sample preparation

The SF solution was prepared following a method outlined in previous studies [24]. First, *bombyx mori* silk cocoons were cut, disposed of the worm, and boiled at 98 °C in a 0.02 M solution of sodium carbonate (Sigma-Aldrich, Cat. No. 451614) water bath to discard sericin. Next, the cocoons were thoroughly washed with distilled water, squeezed to remove excess water, and left to dry overnight. Afterward, SF was dissolved in a 9.3 M solution of lithium bromide (Sigma-Aldrich, Cat. No. 213225) at 60 °C. Salts from the solution were removed by dialyzing with pure water for 48 h. The SF solution was centrifuged at 9000 rpm at 4 °C for 20 min to eliminate aggregates. Finally, the solution was concentrated to 6% w/v by dialyzing with polyethylene glycol (10000 MW, Sigma-Aldrich, Cat. No. P6667). The extracted SF was either used immediately or stored for a short time (less than a week) at 4 °C until required.

The human DCECM powder was obtained from the Royan Institute, Iran. In accordance with an established protocol [25], we performed the enzymatic digestion of DCECM using pepsin. First, 100 mg pepsin (Sigma-Aldrich, Cat. No. 1.07185) was dissolved in 100 ml of 0.01 M hydrochloric acid (Sigma-Aldrich, Cat. No. H9892), forming a digestion solution. Then, 1 g of the DCECM powder was incorporated into the obtained solution and stirred at 4 °C. The enzymatic digestion of DCECM produced a pre-gel solution with a pH of around 3-4. The pH was changed to 7.4 by adding 1 M sodium hydroxide (Sigma-Aldrich, Cat. No.

**This is the accepted manuscript (postprint) of the following article:**
F. Ghanbari, A.H. Taghvaei, E. Salahinejad, M. Pahlevani, Z. Khosrowpour, S.M.A. Haramshahi, M. Gholipourmalekabadi, *Strontium-doped mesoporous bioactive glass reinforced silk fibroin/decellularized extracellular matrix nanocomposite scaffolds for potential bone tissue engineering*, Ceramics International, 51 (2025) 60419-60433.
https://doi.org/10.1016/j.ceramint.2025.10.242

567530) (one-tenth of the initial digest volume) and 10X, phosphate-buffered saline, PBS (one-ninth of the final neutralized volume) [26]. The digested DCECM was carefully transferred into 6-well plates, frozen at -80 °C, lyophilized using a freeze dryer for 24 h, and stored at -80 °C for up to a month until required.

SrMBNs were synthesized using the template-assisted sol-gel method, as described in our previous study [20]. First, polyvinylpyrrolidone (Sigma-Aldrich, Cat. No.234257) and sodium hydroxide (Sigma-Aldrich, Cat. No.221465) were dissolved in 120 ml of pure water. Subsequently, cetyltrimethylammonium bromide (Sigma-Aldrich, Cat. No.H5882) was introduced and mixed for 60 min. Next, a precursor containing calcium nitrate tetrahydrate (Sigma-Aldrich, Cat. No.237124), strontium nitrate (Sigma-Aldrich, Cat. No.243426), and tetraethylorthosilicate (Sigma-Aldrich, Cat. No.131903) were loaded into the solution and mixed for 24 h. The resulting suspension underwent a hydrothermal treatment at 80 °C for 48 h. The obtained gel was rinsed several times with water and ethanol, dried at 100 °C, and lastly calcined at 550 °C for 5 h. Fig. 1 presents the general characteristics of the synthesized SrMBNs. Further details regarding their synthesis and properties can be found in Ref. [20].

**This is the accepted manuscript (postprint) of the following article:**
F. Ghanbari, A.H. Taghvaei, E. Salahinejad, M. Pahlevani, Z. Khosrowpour, S.M.A. Haramshahi, M. Gholipourmalekabadi, *Strontium-doped mesoporous bioactive glass reinforced silk fibroin/decellularized extracellular matrix nanocomposite scaffolds for potential bone tissue engineering*, Ceramics International, 51 (2025) 60419-60433.
https://doi.org/10.1016/j.ceramint.2025.10.242

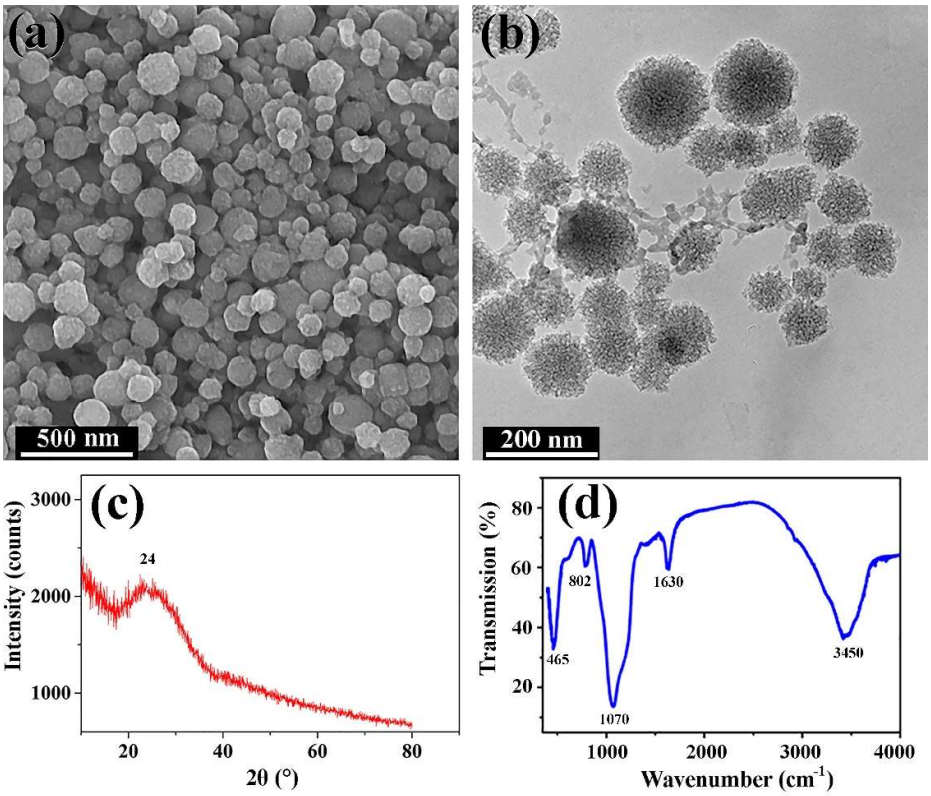


*Fig. 1. Field- emission scanning electron microscopy (FESEM) image (a), transmission electron microscopy (TEM) micrograph (b), X-ray diffraction (XRD) pattern (adapted with permission from Ref. [20]) (c), and Fourier transform infrared spectroscopy (FTIR) spectrum (adapted with permission from Ref. [20]) (d) of the synthesized SrMBNs.*

The lyophilization technique was chosen to fabricate scaffolds. First, the digested DCECM was dissolved in pure water (6 wt%) and then blended to the SF solution in water (6 wt%) for 60 min. The dry-state ratios of SF and DCECM were selected as 100:0, 80:20, 70:30, and 60:40. Afterward, the obtained solution was dispensed into 24-well sterile plates, frozen at -20 °C, and then -80 °C for 24 h. Subsequently, the frozen blends underwent 24 h of lyophilization. For a selected SF/30DCECM (SF with 30 wt% DCECM), the SrMBNs with

**This is the accepted manuscript (postprint) of the following article:**
F. Ghanbari, A.H. Taghvaei, E. Salahinejad, M. Pahlevani, Z. Khosrowpour, S.M.A. Haramshahi, M. Gholipourmalekabadi, *Strontium-doped mesoporous bioactive glass reinforced silk fibroin/decellularized extracellular matrix nanocomposite scaffolds for potential bone tissue engineering*, Ceramics International, 51 (2025) 60419-60433.
https://doi.org/10.1016/j.ceramint.2025.10.242

various concentrations (10, 15, and 20 wt%) were ultrasonically dispersed in the SF/DCECM solution for 30 min and subsequently processed like the SF/DCECM scaffolds. To maintain the integrity of DCECM and prevent the excessive viscosity of SF, all the procedures were conducted at a controlled temperature of 4 °C. Finally, the scaffolds were soaked in 0.5% glutaraldehyde (GLUT) diluted in 96% ethanol for cross-linking, followed by immersion in 1% w/v sodium borohydride for 10 min and subsequently washing with pure water to decrease cytotoxicity caused by the free aldehyde group [27].

## 2-2- Characterization

### 2-2-1- Structure

The pore structure of the specimens was explored by FESEM (QUANTA FEG 450, FEI). The median pore size of the scaffolds was determined from images using ImageJ software. Additionally, energy-dispersive X-ray spectroscopy (EDS, Silicon Drift Detector, 2017), operated at an accelerated voltage of 20 kV, was utilized for quantifying the elemental composition and distribution within the scaffolds.

The functional groups of the scaffolds were studied by attenuated total reflectance-FTIR (ATR-FTIR, Shimadzu). The device was performed on single reflection FTIR with a Near-Infrared DTGS Detector (RX-1, PerkinElmer Spectrum), within a wavenumber range of 4000 to 400 $cm^{-1}$ at a resolution of 1 $cm^{-1}$. The crystallinity index (*CI*%) was calculated from the ATR-FTIR spectra, as the intensity ratio of peaks at wavenumbers 1260 and 1235 $cm^{-1}$ in the ATR-FTIR spectra, using the following equation [28]:

$$CI\% = \frac{A\ 1260\ cm^{-1}}{A\ 1235\ cm^{-1}} \times 100 \quad (1)$$

**This is the accepted manuscript (postprint) of the following article:**
F. Ghanbari, A.H. Taghvaei, E. Salahinejad, M. Pahlevani, Z. Khosrowpour, S.M.A. Haramshahi, M. Gholipourmalekabadi, *Strontium-doped mesoporous bioactive glass reinforced silk fibroin/decellularized extracellular matrix nanocomposite scaffolds for potential bone tissue engineering*, Ceramics International, 51 (2025) 60419-60433.
https://doi.org/10.1016/j.ceramint.2025.10.242

where $A1235\ \mathrm{cm}^{-1}$ and $A1260\ \mathrm{cm}^{-1}$ are absorbance at 1235 and 1260 $\mathrm{cm}^{-1}$, respectively. FTIR band deconvolution was performed using the XPSPEAK41 software with Gaussian functions.

The porosity of the scaffolds was determined using the liquid displacement method, which relies on the Archimedes' principle. To avoid potential swelling or shrinking effects caused by ethanolic solutions, hexane was chosen as a non-solvent liquid. The dry specimens were weighed ($w_d$), immersed in hexane for 5 min, and then weighed while suspended in hexane ($w_l$). Then, after wiping off excess hexane from the surfaces using a filter paper, the wet scaffolds were weighed ($w_w$) and their porosity was calculated as below:

$$\text{Porosity } (\%) = (w_w - w_d)/(w_w - w_l) \times 100 \quad (2)$$

### 2-2-2- Biomechanical properties

The biomechanical behavior of the scaffolds was studied by compression testing, following the modified version of the ASTM D695-15 (ISO 604) standard, using a Hounsfield-H25KS testing machine. Standard cylindrical-shaped scaffolds with a height to diameter ratio of 2 were used. The scaffolds were compressed using a 500 N load cell, resulting in approximately 70% reduction of their initial length with the force increased at a rate of 0.5 mm/min.

**This is the accepted manuscript (postprint) of the following article:**
F. Ghanbari, A.H. Taghvaei, E. Salahinejad, M. Pahlevani, Z. Khosrowpour, S.M.A. Haramshahi, M. Gholipourmalekabadi, *Strontium-doped mesoporous bioactive glass reinforced silk fibroin/decellularized extracellular matrix nanocomposite scaffolds for potential bone tissue engineering*, Ceramics International, 51 (2025) 60419-60433.
https://doi.org/10.1016/j.ceramint.2025.10.242

### 2-2-3- Swelling and degradation kinetics

The swelling properties of the scaffolds were studied following the literature [29]. First, the same size cylindrical scaffolds were weighed ($T_d$) and soaked in PBS for various time intervals at 37 °C. After reaching swelling equilibrium, the scaffolds were removed and excess PBS on the surface was wiped off using a filter paper. Subsequently, the scaffolds were re-weighed ($T_s$). Finally, their swelling ratio was calculated as following:

$$\text{Swelling ratio} = (T_s - T_d)/T_d \quad (3)$$

The ASTM F1635-11 standard test method was employed to measure the degradation rate of the specimens. First, the samples with the dimensions of 1×1×1 $cm^3$ were freeze-dried, weighed ($w_0$), and immersed in PBS (pH 7.4, at 37 °C) for 3, 7, 10, 14, and 21 days. Then, they were taken out of PBS and washed with water. After drying in a lab oven for a day (37 °C), they were weighed again ($w_d$). Finally, the degradation rate of the specimens was determined as below:

$$\text{Degradation rate (\%)} = (w_0 - w_d)/w_0 \times 100 \quad (4)$$

### 2-2-4- Apatite-formation ability

The *in-vitro* apatite formation of the scaffolds was evaluated, following the international standard ISO 23317:2025. First, the specimens were soaked in SBF at various time intervals in an incubator (37 °C). Then, the scaffolds were removed from the solution and after gently rinsing with pure water and drying, the scaffolds were analyzed via FESEM and FTIR techniques. To further study the bioactivity of the samples, the release of $Ca^{2+}$ in SBF was examined by inductively coupled plasma optical emission spectroscopy (ICP-OES, Optima

**This is the accepted manuscript (postprint) of the following article:**
F. Ghanbari, A.H. Taghvaei, E. Salahinejad, M. Pahlevani, Z. Khosrowpour, S.M.A. Haramshahi, M. Gholipourmalekabadi, *Strontium-doped mesoporous bioactive glass reinforced silk fibroin/decellularized extracellular matrix nanocomposite scaffolds for potential bone tissue engineering*, Ceramics International, 51 (2025) 60419-60433.
https://doi.org/10.1016/j.ceramint.2025.10.242

7300 DV, PerkinElmer) and the mass changes of the scaffold during time intervals of soaking in SBF was studied.

### 2-2-5- Cell viability

The viability of rat bone marrow mesenchymal stem cells (rBMSCs) cultured on the scaffolds was measured by the MTT assay. For this purpose, $2\times1\times1$ $mm^3$ scaffolds were sterilized under a 15W UV light for 60 min and then transferred into a 96-well culture plate, with scaffold-free wells serving as the control. Subsequently, they were rinsed with PBS and incubated with Dulbecco's Modified Eagle's Medium (DMEM)/F-12 at 37 °C overnight. Next, $3\times10^3$ cells were seeded onto each scaffold and placed in an incubator under cell culture conditions (95% humidity, 5% $CO_2$, and temperature of 37 °C). After 1, 3, and 7 days, the culture medium was discarded, and 100 µl MTT solution was introduced to each scaffold. Following 4 h of incubation, the MTT solution was aspirated, and 100 µl dimethyl sulfoxide (DMSO) was added to each scaffold. After 15 min of shaking, an ELISA reader (Dynex Technologies) was employed to measure the absorption of the scaffolds.

### 2-2-6- Cell adhesion

The rBMSCs morphology and adhesion on the scaffolds were investigated by FESEM. First, 1 $cm^2$ of each scaffold was seeded with $3\times10^3$ rBMSCs and kept under the cell culture conditions for 48 h. Next, the scaffolds were taken out and fixed in 2.5% v/v GLUT in PBS for 2 h. Then, they were rinsed three times with PBS and water. To dehydrate the scaffolds and

**This is the accepted manuscript (postprint) of the following article:**
F. Ghanbari, A.H. Taghvaei, E. Salahinejad, M. Pahlevani, Z. Khosrowpour, S.M.A. Haramshahi, M. Gholipourmalekabadi, *Strontium-doped mesoporous bioactive glass reinforced silk fibroin/decellularized extracellular matrix nanocomposite scaffolds for potential bone tissue engineering*, Ceramics International, 51 (2025) 60419-60433.
https://doi.org/10.1016/j.ceramint.2025.10.242

remove residual water, a series of alcohol solutions with increasing concentrations (30, 50, 70, and 100%) was used, and the scaffolds were then air-dried.

### 2-2-7- Osteogenic potential

The production of mineralized calcium was used as a marker of osteogenic differentiation using Alizarin Red S (ARS) staining [30]. First, $30\times10^3$ rBMSCs were seeded in DMEM/F-12 medium with 10% fetal bovine serum (FBS), 100 U penicillin, and 100 µg streptomycin within a 6-well plate under cell culture conditions. Following 24 h, the scaffolds were introduced into the plates, and the DMEM/F-12 medium was replaced with the differentiation medium containing low-glucose DMEM, 10% FBS, 50 mM ascorbate-2-phosphate, 1% penicillin/streptomycin, 100 nM dexamethasone, and 10 mM glycerol-phosphate. After 14 days of incubation, with the medium change every 3 days, the cells were analyzed for the development of the mineralized bone matrix. For this purpose, the scaffolds were taken out of the media and the cells were rinsed with PBS. Then, the cells were fixed in 4% formalin for 10 min at 25 °C and rinsed with pure water. Next, the cells were exposed to a 2% ARS solution in PBS at 25 °C for 30 min, followed by pH adjustment at 4.1-4.3 using ammonium hydroxide. Finally, the amount of mineralization was measured using 20% methanol and 10% acetic acid and the absorbance of the samples was read by a spectrophotometer (Pharmacia Biotech).

### 2-2-8- Statistical analysis

All measurements were conducted in triplicate ($n$ = 3) and are presented as mean ± standard deviation (SD), with SDs specified by error bars in charts. Statistical comparisons

**This is the accepted manuscript (postprint) of the following article:**
F. Ghanbari, A.H. Taghvaei, E. Salahinejad, M. Pahlevani, Z. Khosrowpour, S.M.A. Haramshahi, M. Gholipourmalekabadi, *Strontium-doped mesoporous bioactive glass reinforced silk fibroin/decellularized extracellular matrix nanocomposite scaffolds for potential bone tissue engineering*, Ceramics International, 51 (2025) 60419-60433.
https://doi.org/10.1016/j.ceramint.2025.10.242

were performed using one-way analysis of variance (ANOVA), with $p < 0.05$ considered statistically significant, using the SPSS software.

## 3- Results and discussion

### 3-1- Morphological characterization

The formation of a porous structure in tissue-engineering scaffolds is crucial for improving cell attachment, proliferation, and differentiation, while the interconnectedness of pores facilitates nutrient delivery and waste removal for cells within the scaffolds [31]. From this perspective, the undesirable lamellar structure of pure SF accompanied by a reduced surface area is revealed in Fig. 2, which can limit cell interactions. Prior studies [32, 33] have indicated that incorporating additives like collagen and gelatin can disrupt the lamellar formation of SF, suggesting that DCECM could induce a similar beneficial restructuring, as verified by our results. Specifically, in the SF/20DCECM scaffold, a porous structure with thin walls separating pores was successfully developed through the freeze-drying method. In the SF/40DCECM scaffold, despite the achievement of a completely formed porous structure, most pores are blocked due to the excessive content of DCECM. In contrast, the SF/30DCECM scaffold demonstrates a remarkably interconnected porous structure, with no discernible remnants of the lamellar structure of SF. This formulation was selected as optimal for SrMBNs reinforcement, as confirmed by its suitable pore size, porosity, and superior mechanical performance (Section 3.3).

**This is the accepted manuscript (postprint) of the following article:**
F. Ghanbari, A.H. Taghvaei, E. Salahinejad, M. Pahlevani, Z. Khosrowpour, S.M.A. Haramshahi, M. Gholipourmalekabadi, *Strontium-doped mesoporous bioactive glass reinforced silk fibroin/decellularized extracellular matrix nanocomposite scaffolds for potential bone tissue engineering*, Ceramics International, 51 (2025) 60419-60433.
https://doi.org/10.1016/j.ceramint.2025.10.242

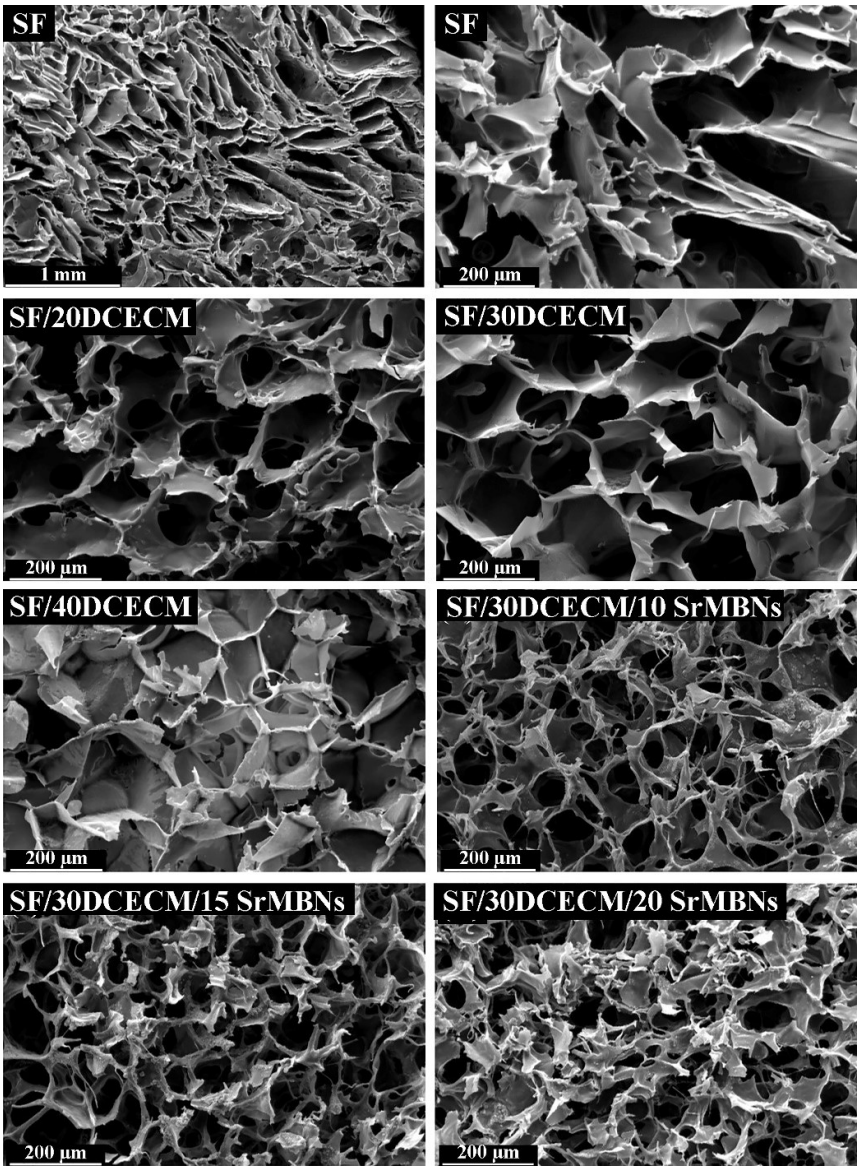


*Fig. 2. SEM images of the produced scaffolds.*

Fig. 2 also shows the influence of the SrMBN addition on the morphology of the scaffolds. The porous morphology is preserved for SF/30DCECM with 10% SrMBNs, but with an irregular distribution of the SrMBNs. Also, a non-uniform distribution of SrMBNs, collapse of the pore walls, and loss of the porous structure are caused by an excessive addition of the

**This is the accepted manuscript (postprint) of the following article:**
F. Ghanbari, A.H. Taghvaei, E. Salahinejad, M. Pahlevani, Z. Khosrowpour, S.M.A. Haramshahi, M. Gholipourmalekabadi, *Strontium-doped mesoporous bioactive glass reinforced silk fibroin/decellularized extracellular matrix nanocomposite scaffolds for potential bone tissue engineering*, Ceramics International, 51 (2025) 60419-60433.
https://doi.org/10.1016/j.ceramint.2025.10.242

SrMBNs, as evident in SF/30DCECM with 20% SrMBNs. However, the SF/30DCECM/15SrMBNs scaffold exhibits a complex and interconnected porous structure with a uniform distribution of the SrMBNs on the surface of the pore walls and increased surface roughness, which are beneficial for cell attachment, growth, and differentiation. The EDS mapping analysis of this optimal scaffold reveals a homogenous elemental distribution, as depicted in Fig. 3(a, b), pivotal for the scaffold's consistent biomechanical and biological behaviors.

**This is the accepted manuscript (postprint) of the following article:**
F. Ghanbari, A.H. Taghvaei, E. Salahinejad, M. Pahlevani, Z. Khosrowpour, S.M.A. Haramshahi, M. Gholipourmalekabadi, *Strontium-doped mesoporous bioactive glass reinforced silk fibroin/decellularized extracellular matrix nanocomposite scaffolds for potential bone tissue engineering*, Ceramics International, 51 (2025) 60419-60433.
https://doi.org/10.1016/j.ceramint.2025.10.242

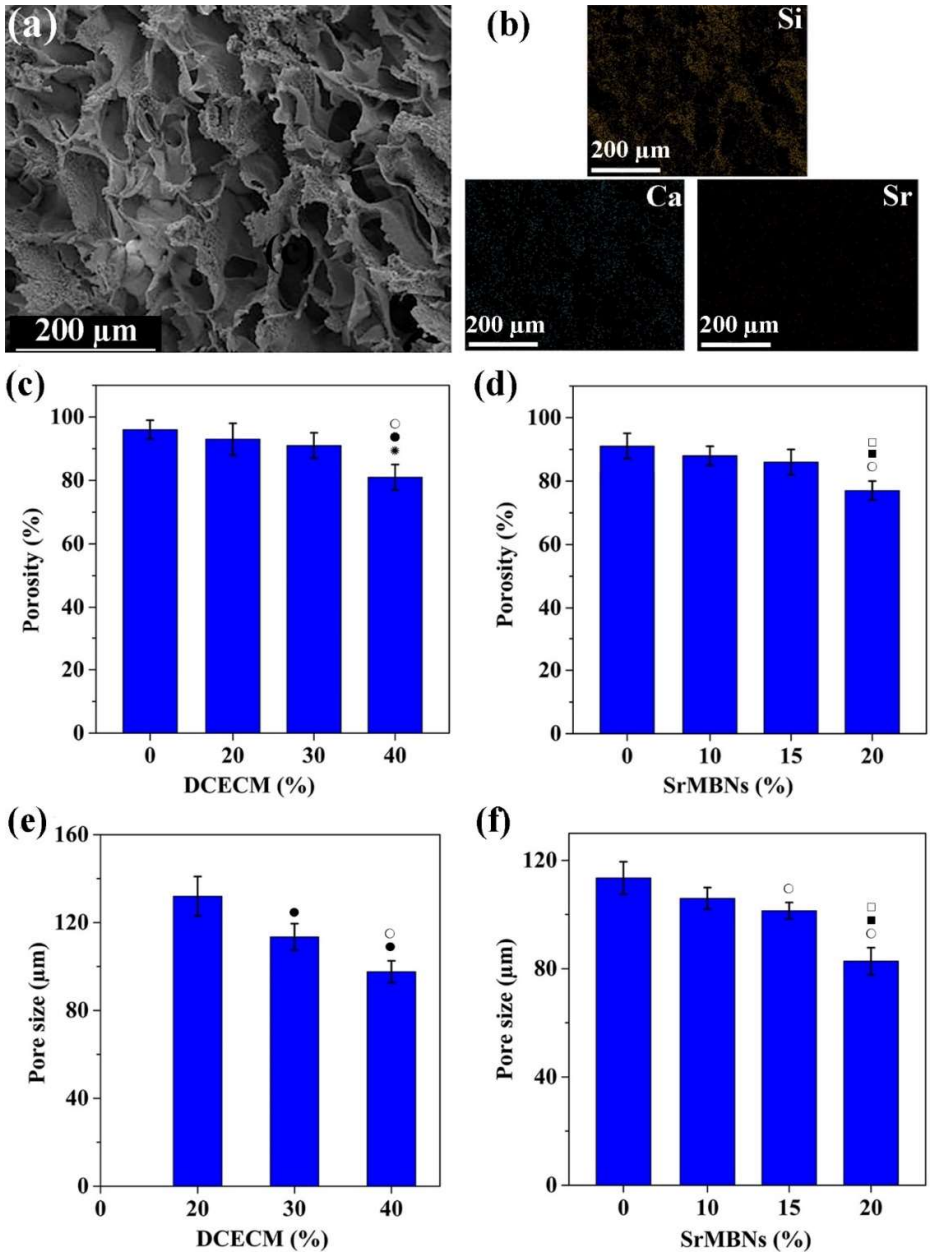


*Fig. 3. SEM image (a) and corresponding EDS mapping (b) of the SF/30DCECM/15 SrMBNs scaffold, effects of the DCECM and SrMBNs additions on the porosity of the SF/DCECM (c) and SF/30DCECM/SrMBNs scaffolds (d), and influences of the DCECM (e) and SrMBN (f) additions on the pore size of the SF/30DCECM/SrMBNs scaffolds (*, ●, ○, ■, and □ denote significant differences relative to the SF, SF/20DCECM, SF/30DCECM, SF/30DCECM/10 SrMBNs, and SF/30DCECM/15 SrMBNs samples in each chart, respectively, with $p < 0.05$).*

**This is the accepted manuscript (postprint) of the following article:**
F. Ghanbari, A.H. Taghvaei, E. Salahinejad, M. Pahlevani, Z. Khosrowpour, S.M.A. Haramshahi, M. Gholipourmalekabadi, *Strontium-doped mesoporous bioactive glass reinforced silk fibroin/decellularized extracellular matrix nanocomposite scaffolds for potential bone tissue engineering*, Ceramics International, 51 (2025) 60419-60433.
https://doi.org/10.1016/j.ceramint.2025.10.242

Fig. 3 also depicts the influence of the DCECM and SrMBN additions on the porosity of the prepared scaffolds. As can be seen, the mean porosity of SF is gradually reduced from 96 to 81% by the addition of DCECM (Fig. 3(c)). The results suggest that incorporating 20 and 30% DCECM into the SF scaffold did not lead to a significant alteration in porosity, while a reduction of approximately 15% in porosity was observed with the addition of 40% DCECM, which is in agreement with Fig. 2. One plausible explanation for this observation is interactions between DCECM and SF, which could influence the scaffold's pore structure, prompting a transition from a lamellar to a porous structure, increasing density, and consequently lowering porosity. The same trend is observed upon the addition of the SrMBNs to the SF/30DCECM scaffold (Fig. 3(d)). In this case, the mean porosity of the scaffolds is declined from 91 to 88, 86, and 77% by incorporating 10, 15, and 20% SrMBNs, respectively. The results suggest that incorporating 10 or 15% SrMBNs into the SF/30DCECM scaffold did not significantly change its porosity, whereas adding 20% resulted in a considerable reduction of approximately 13%. As shown in Fig. 2, the excessive addition of the SrMBNs can destroy the inner structure of the scaffolds.

The pore size of a scaffold should be small enough to maintain mechanical integrity and sufficiently large to support nutrient and waste diffusion. It has been found that pore sizes smaller than 100 μm may not be sufficient for mass transport and cell migration, potentially leading to premature endochondral cartilage formation before osteogenesis [31, 34]. While the pore size is not typically reported for lamellar structures including SF scaffolds, the addition of DCECM gave rise to a significant decrease in the pore size of the SF/DCECM scaffold. Specifically, the mean pore size decreased from 132 μm in the SF/20DCECM scaffold to 114

**This is the accepted manuscript (postprint) of the following article:**
F. Ghanbari, A.H. Taghvaei, E. Salahinejad, M. Pahlevani, Z. Khosrowpour, S.M.A. Haramshahi, M. Gholipourmalekabadi, *Strontium-doped mesoporous bioactive glass reinforced silk fibroin/decellularized extracellular matrix nanocomposite scaffolds for potential bone tissue engineering*, Ceramics International, 51 (2025) 60419-60433.
https://doi.org/10.1016/j.ceramint.2025.10.242

μm and 98 μm with 30 and 40% DCECM, respectively, as indicated in Fig. 3(e). Despite the notable decrease in the pore size with increasing the DCECM content, the scaffold pore size remained within an acceptable range, except for the SF/40DCECM sample. Based on Fig. 3(f), by introducing the SrMBNs into the SF/30DCECM scaffold, a reduction in the mean pore size to 106, 101, and 83 μm for 10, 15, and 20% SrMBN additions, respectively, was obtained. These configurations promise to offer a well-balanced architecture for effective cell activities and tissue regeneration.

### 3-2- Chemical analysis

The FTIR spectra of the SF, SF/30DCECM, and SF/30DCECM/15SrMBNs scaffolds after cross-linking are shown in Fig. 4a. By adding DCECM to SF, blue shifts in the characteristic peaks of amides—amide I (C=O stretching at 1600-1800 $cm^{-1}$), amide II (N-H bending at 1470-1570 $cm^{-1}$), amide III (C-N stretching at 1250-1350 $cm^{-1}$), and amide A (N-H stretching at 3300-3500 $cm^{-1}$) [35]—are observed. The observed shifts, particularly in the amide I band, suggest strengthening of the carbonyl bond. This likely originates from competitive hydrogen bonding, wherein hydrophilic DCECM components (e.g., hydroxyl groups) interact with the C=O bond of SF. By forming stronger hydrogen bonds, the increase in the electron density withdrawal from the carbonyl group strengthens the C=O bond, causing a blue shift. In contrast, the addition of 15% SrMBNs to the SF/30DCECM scaffold led to red shifts in the characteristic peaks of the amides. This is because the dissolution products of bioactive glass, such as $Ca^{2+}$, can coordinate with the carboxylic groups of proteins [36]. This

**This is the accepted manuscript (postprint) of the following article:**
F. Ghanbari, A.H. Taghvaei, E. Salahinejad, M. Pahlevani, Z. Khosrowpour, S.M.A. Haramshahi, M. Gholipourmalekabadi, *Strontium-doped mesoporous bioactive glass reinforced silk fibroin/decellularized extracellular matrix nanocomposite scaffolds for potential bone tissue engineering*, Ceramics International, 51 (2025) 60419-60433.
https://doi.org/10.1016/j.ceramint.2025.10.242

chelation could contribute to the ionic bridging between protein chains [37], which could impose constraint on the C=O bonds, causing them to vibrate at a lower frequency.

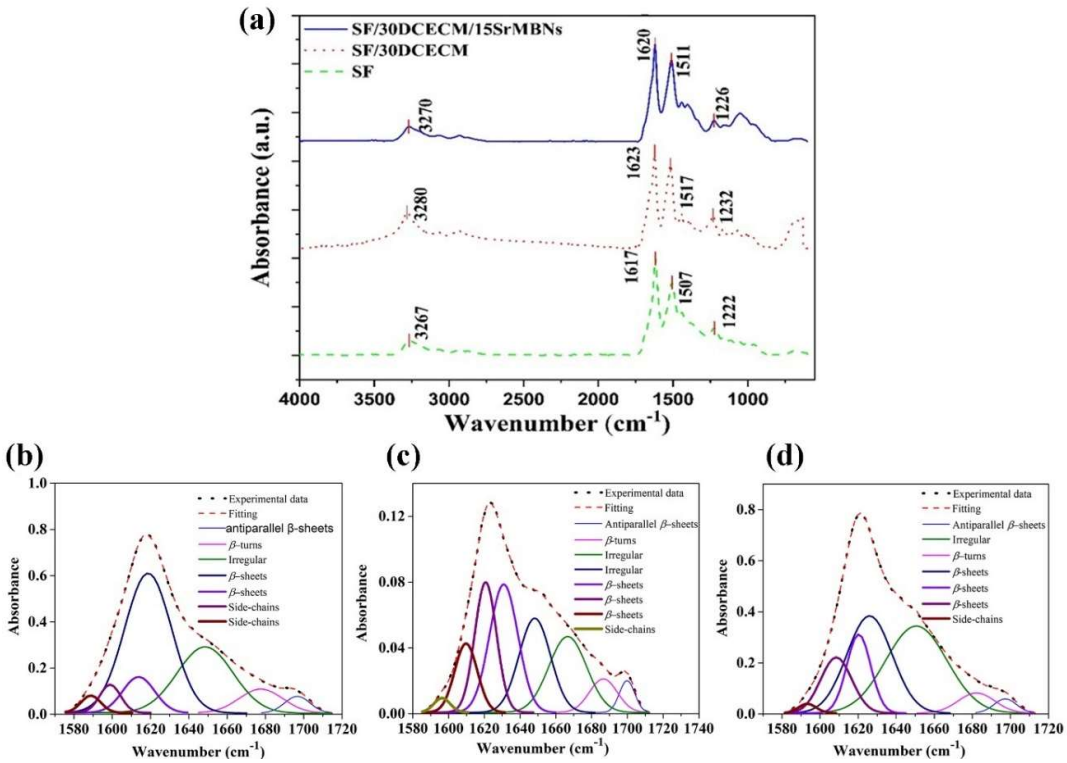


*Fig. 4. FTIR spectra of the produced scaffolds (a), and deconvoluted amide I region for the SF (b), SF/30DCECM (c), and SF/30DCECM/15SrMBNs (d) samples.*

The SF scaffold exhibits the highest *CI* of 81.12 %, as calculated by Eq. 1, indicative of its superior crystallization. This highest crystallinity likely stems from self-assembly and strong hydrogen bonding among SF chains, fostering the creation of highly crystalline *β*-sheet structures. In contrast, the SF/30DCECM scaffold displays a slightly diminished *CI* of 78.48%, suggesting a marginally reduced crystallization of SF. In contrast, the SF/30DCECM/15SrMBNs scaffold shows the lowest *CI* of 62.4%, signifying the least

**This is the accepted manuscript (postprint) of the following article:**
F. Ghanbari, A.H. Taghvaei, E. Salahinejad, M. Pahlevani, Z. Khosrowpour, S.M.A. Haramshahi, M. Gholipourmalekabadi, *Strontium-doped mesoporous bioactive glass reinforced silk fibroin/decellularized extracellular matrix nanocomposite scaffolds for potential bone tissue engineering*, Ceramics International, 51 (2025) 60419-60433.
https://doi.org/10.1016/j.ceramint.2025.10.242

crystallization of SF. The impact of DCECM and subsequent SrMBNs on the secondary structure of SF was further assessed by deconvoluting the amide I region of the FTIR spectra into multiple Gaussian peaks to fit the experimental data (Figs. 4(b-d)). Accordingly, peaks below 1600 $cm^{-1}$ were attributed to amino acid side-chain vibrations [38]. Peaks between 1610–1630 $cm^{-1}$ and around 1700 $cm^{-1}$ were assigned to $\beta$-sheet and antiparallel $\beta$-sheet structures, respectively [38,39]. Peaks in the central amide I region (approximately 1650–1660 $cm^{-1}$) were attributed to random coil (irregular) conformations, while the peak at 1680 $cm^{-1}$ was assigned to $\beta$-turn structures [38, 40]. The fraction of each secondary structure was calculated by integrating the area of its corresponding Gaussian peak and dividing by the total integrated area of the amide I band, as summarized in Table 1. The SF scaffold exhibited the highest $\beta$-sheet content (57%), indicating a high crystallinity, which is consistent with its high *CI*. The addition of 30% DCECM reduced the $\beta$-sheet content to 53% and increased the random coil content from 26 to 35%. This decrease in the structural order is consistent with a lower *CI* and suggests that DCECM components competitively interact with the SF backbone. This interaction, as supported by the blue shift in the amide I frequency, disrupts the native inter-chain hydrogen bonding that is vital for the formation and stability of the $\beta$-sheet crystals. This result is accompanied by the reduction of the $\beta$-sheet fraction and increased random coil component, confirming the impeding effect of DCECM on the long-range self-assembly of $\beta$-sheets. In contrast, based on Table 1, no more variations in fractions of the $\beta$-sheet or random coil structure are observed after the incorporation of SrMBNs, indicating that the nanoparticles do not alter quantitatively the second structure of SF. However, a notable decrease of *CI* to 62.4 % suggests that SrMBNs can act as a physical barrier that prevents the effective alignment and long-range packing of the $\beta$-sheet regions. Furthermore, the aforementioned bridging effect

**This is the accepted manuscript (postprint) of the following article:**
F. Ghanbari, A.H. Taghvaei, E. Salahinejad, M. Pahlevani, Z. Khosrowpour, S.M.A. Haramshahi, M. Gholipourmalekabadi, *Strontium-doped mesoporous bioactive glass reinforced silk fibroin/decellularized extracellular matrix nanocomposite scaffolds for potential bone tissue engineering*, Ceramics International, 51 (2025) 60419-60433.
https://doi.org/10.1016/j.ceramint.2025.10.242

of $Ca^{2+}$ possibly contributes to suppressed *CI* via local cross-linking at some points, which could frustrate a long-range rearrangement required for the formation of a highly crystalline structure.

*Table 1. Fractional content of secondary structure components for the difference scaffolds.*

| Sample | *β*-sheets (%) | *β*-turns (%) | Irregular (%) |
|---|---|---|---|
| **SF** | 57 | 17 | 26 |
| **SF-30% DCECM** | 54 | 11 | 35 |
| **SF-30% DCECM-15% SrMBNs** | 53 | 11 | 36 |

### 3-3- Mechanical properties

Fig. 5(a) depicts the stress-strain curve of the SF/DCECM scaffolds with the different DCECM contents. Furthermore, the extracted values of compressive strength and elastic modulus are represented in Figs. 5(b) and (c), respectively. The results show that by adding DCECM up to 30%, the mean compressive strength and elastic modulus increase from 137 to 403 kPa, and 165 to 520 kPa, respectively. In contrast, the excessive addition of DCECM to SF (40%) is followed by a notable decrease of both compressive strength and elastic modulus. These findings suggest that there is an optimal ratio of DCECM (30%) addition to SF, which can achieve the highest compressive strength and elastic modulus. The possible explanation

**This is the accepted manuscript (postprint) of the following article:**
F. Ghanbari, A.H. Taghvaei, E. Salahinejad, M. Pahlevani, Z. Khosrowpour, S.M.A. Haramshahi, M. Gholipourmalekabadi, *Strontium-doped mesoporous bioactive glass reinforced silk fibroin/decellularized extracellular matrix nanocomposite scaffolds for potential bone tissue engineering*, Ceramics International, 51 (2025) 60419-60433.
https://doi.org/10.1016/j.ceramint.2025.10.242

for increasing the compressive strength and elastic modulus of the scaffolds by adding DCECM is interactions between DCECM and SF, which transforms the lamellar structure pf SF into the porous one, as confirmed by the FESEM images earlier (Fig. 2). On the contrary, the reduction in compressive strength and elastic modulus with the excessive addition of DCECM can stem from the inherently weaker mechanical properties of DCECM in comparison to SF.

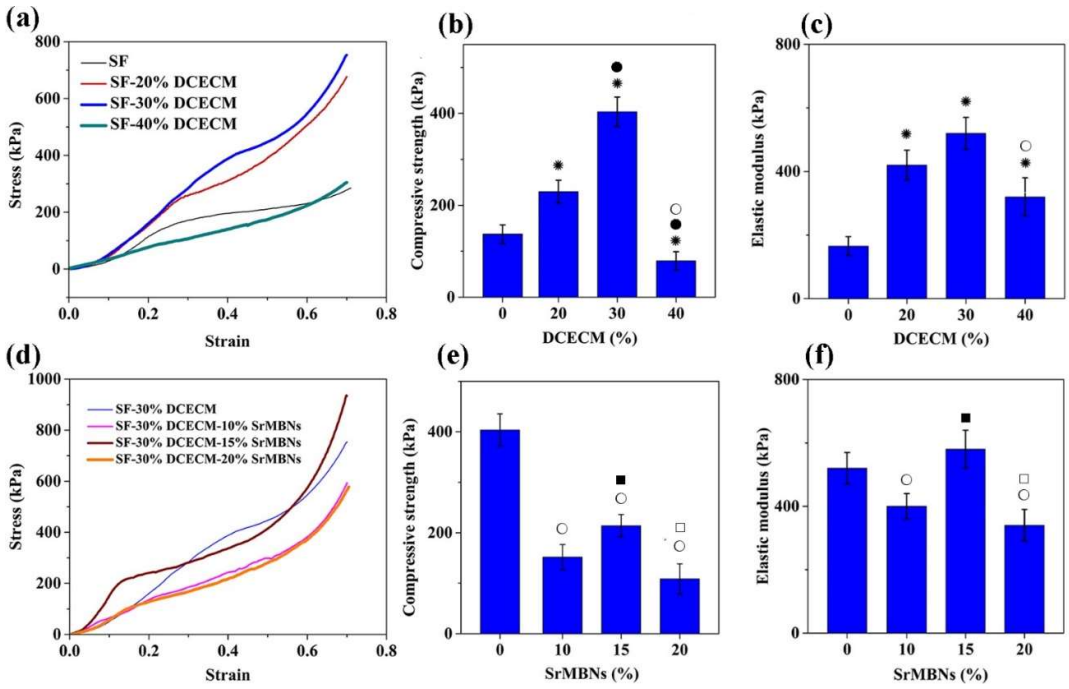


*Fig. 5. Compressive stress-strain plots (a), compressive strength (b), and elastic modulus (c) of the SF/DCECM scaffolds, along with compressive stress-strain plots (d), compressive strength (e), and elastic modulus (f) of the SF/30DCECM/SrMBNs scaffolds (*, ●, ○, ■, and □ denote significant differences relative to the SF, SF/20DCECM, SF/30DCECM, SF/30DCECM/10 SrMBNs, and SF/30DCECM/15 SrMBNs scaffolds in each chart, respectively, with $p < 0.05$).*

Fig. 5(d) illustrates the stress-strain plots of the SF/30DCECM scaffolds following the incorporation of the varying SrMBNs contents. In each plot, an initial elastic distortion is

**This is the accepted manuscript (postprint) of the following article:**
F. Ghanbari, A.H. Taghvaei, E. Salahinejad, M. Pahlevani, Z. Khosrowpour, S.M.A. Haramshahi, M. Gholipourmalekabadi, *Strontium-doped mesoporous bioactive glass reinforced silk fibroin/decellularized extracellular matrix nanocomposite scaffolds for potential bone tissue engineering*, Ceramics International, 51 (2025) 60419-60433.
https://doi.org/10.1016/j.ceramint.2025.10.242

observed in small strains, accompanied by the collapse of cell walls. Subsequently, there is a rapid increase in stress, attributed to the densification of the porous structure [41]. Based on Fig. 5(e), the scaffold without the SrMBNs shows the highest compressive strength, whereas the SF/DCECM scaffold with 15% SrMBNs displays the maximum elastic modulus among all the prepared specimens (Fig. 5(f)). Additionally, the latter sample demonstrates the largest compressive strength among the SrMBN-loaded scaffolds. The negative effect of the excessive addition of the SrMBNs (beyond 15%) on the mechanical behaviors can be associated with less uniform scaffold morphology (refer to Fig. 2). Furthermore, a high tendency of the SrMBNs for agglomeration may lead to the formation of nanovoids, contributing to increased brittleness and decreased compressive strength compared to the SrMBN-free SF/DCECM scaffolds. The lower elastic modulus of the scaffolds containing 10% SrMBNs compared to the SF/30% DCECM scaffold (Fig. 5(g)) is consistent with a disruptive role of the nanoparticles in the formation of well-ordered, rigid crystalline domains, as evidenced by the decreased *CI* values. In other words, the loss of long-range, high-stiffness crystalline structure reduces the inherent stiffness of the matrix. At 10% SrMBNs loading, this weakening effect outweighs the particles' reinforcing contribution. However, increasing the SrMBN content to 15% significantly increases the elastic modulus, suggesting an optimum concentration was obtained where the SrMBNs form a continuous, load-bearing network. The subsequent modulus decrease at 20% loading likely results from agglomeration and structural defects caused by exceeding the optimal filler content. Despite a decrease in compressive strength due to the SrMBNs incorporation, the SF/DCECM/15%SrMBNs scaffold, while not directly equivalent to natural bone, exhibits significantly superior mechanical properties compared to the SF scaffold.

**This is the accepted manuscript (postprint) of the following article:**
F. Ghanbari, A.H. Taghvaei, E. Salahinejad, M. Pahlevani, Z. Khosrowpour, S.M.A. Haramshahi, M. Gholipourmalekabadi, *Strontium-doped mesoporous bioactive glass reinforced silk fibroin/decellularized extracellular matrix nanocomposite scaffolds for potential bone tissue engineering*, Ceramics International, 51 (2025) 60419-60433.
https://doi.org/10.1016/j.ceramint.2025.10.242

### 3-4- Swelling behavior

The swelling ability of scaffolds is a critical factor for maintaining structural stability and facilitating cell diffusion. It modifies the nutrition and waste transport rate, and controls protein adsorption, cell attachment, and proliferation [42]. However, if a scaffold absorbs an excessive amount of water, it may lose its shape and strength. Therefore, it is essential to optimize the swelling ability of the scaffolds. As shown in Fig. 6(a), the swelling ratio of the scaffolds increased continuously within 30 min of soaking in PBS, reaching mean values of 7.2 for SF and 10.3, 11.5, and 13.2 for the scaffolds with 20, 30, and 40% DCECM, respectively. After that, the swelling ratio remained constant in all the groups. Indeed, the addition of DCECM to the SF matrix increases notably the swelling ratio of the composite scaffolds, due to a more hydrophilic nature of DCECM compared to SF. In contrast to DCECM, the addition of the SrMBNs has a slightly negative effect on the swelling behavior of the scaffolds. Fig. 6(b) shows that the swelling ratio of the scaffolds increased within 30 min of soaking in PBS and then stabilized, reaching average values of 11, 10.6, and 9.8 for the scaffolds with 10, 15, and 20% SrMBNs, respectively. Indeed, the SrMBN addition to SF/30DCECM is followed by a reduced average pore size as well as porosity of the scaffolds (Fig. 2), leading to a suppressed swelling ratio. Another possible explanation could be interactions between the SrMBNs and DCECM, which lowers the number of available hydrophilic sites in the scaffold [42]. These results suggest that the decrease in the swelling ratio observed in the optimized SrMBNs-incorporated scaffold (SF/30DCECM/15SrMBNs) is minor, where this scaffold still exhibits a significantly improved swelling behavior compared to pure SF.

**This is the accepted manuscript (postprint) of the following article:**
F. Ghanbari, A.H. Taghvaei, E. Salahinejad, M. Pahlevani, Z. Khosrowpour, S.M.A. Haramshahi, M. Gholipourmalekabadi, *Strontium-doped mesoporous bioactive glass reinforced silk fibroin/decellularized extracellular matrix nanocomposite scaffolds for potential bone tissue engineering*, Ceramics International, 51 (2025) 60419-60433.
https://doi.org/10.1016/j.ceramint.2025.10.242

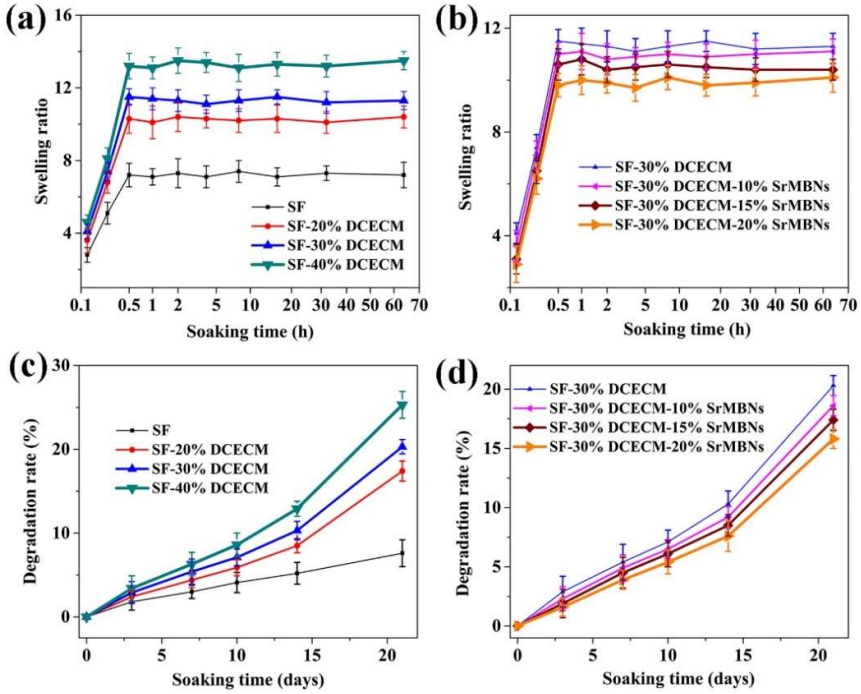


*Fig. 6. Swelling ratio of the SF/DCECM (a) and SF/30DCECM/SrMBNs (b)scaffolds, as well as degradation rate of the SF/DCECM (c) and SF/30DCECM/SrMBNs (d) samples.*

### 3-5- Degradation rate

The degradation rate of a scaffold is one of the key factors that influences its performance after implantation into the patient's body. The scaffold should degrade at a rate that matches the tissue regeneration rate, so that it can offer a sufficient biomechanical support for the new tissue and also allow enough space for the bone growth [43]. As shown in Fig. 6(c), the degradation rate of the scaffolds increases steadily within 21 days of soaking in PBS. Specifically, the mean value of 7.6% was observed for SF, while in the scaffolds containing 20, 30, and 40% DCECM, the values were 17.4, 20.3, and 25.3%, respectively. The enhanced degradation of the scaffolds after the DCECM addition is in line with the improved swelling

**This is the accepted manuscript (postprint) of the following article:**
F. Ghanbari, A.H. Taghvaei, E. Salahinejad, M. Pahlevani, Z. Khosrowpour, S.M.A. Haramshahi, M. Gholipourmalekabadi, *Strontium-doped mesoporous bioactive glass reinforced silk fibroin/decellularized extracellular matrix nanocomposite scaffolds for potential bone tissue engineering*, Ceramics International, 51 (2025) 60419-60433.
https://doi.org/10.1016/j.ceramint.2025.10.242

ratio, as well as the higher degradation rate of collagen as the main component of DCECM compared to SF. On the other hand, the SrMBNs concentration had an inverse effect on the weight loss of the SF/30DCECM scaffold. Fig. 6(d) demonstrates that after 21 days of immersion in PBS, the degradation rate of the SrMBNs-incorporated scaffolds reached mean values of 18.6, 17.4, and 15.8% for the scaffolds with 10, 15, and 20% SrMBNs, respectively. The decrease in the degradation rate after the SrMBNs addition can be attributed to several factors, including the diminished swelling ratio, porosity, and pore size, particularly for the high SrMBNs contents, as discussed earlier. Additionally, a more chemically stable network is expected due to interactions of the SrMBNs with components of DCECM, specifically collagen, which could physically protect collagen or other ECM components against hydrolytic cleavage. Furthermore, a lower weight loss of the SrMBNs-incorporated scaffolds may stem from a lower dissolution rate of the SrMBNs compared to DCECM. These results demonstrate that by incorporating the SrMBNs into the SF/30DCECM scaffold, the degradation rate can be modulated and optimized for a long-term use. This is advantageous because it can allow sufficient time for ECM formation during *in-vivo* bone tissue regeneration, as supported by the literature [43].

### 3-6- Apatite formation ability *in-vitro*

*In-vitro* bioactivity is the ability of biomaterials to produce an apatite layer in SBF. It is a reliable method to estimate how a biomaterial will bond to living bone tissue [44]. The apatite layer is capable of connecting the biomaterial and tissue with attracting growth factors and serum proteins, which are important for cell attachment and subsequent differentiation [16].

**This is the accepted manuscript (postprint) of the following article:**
F. Ghanbari, A.H. Taghvaei, E. Salahinejad, M. Pahlevani, Z. Khosrowpour, S.M.A. Haramshahi, M. Gholipourmalekabadi, *Strontium-doped mesoporous bioactive glass reinforced silk fibroin/decellularized extracellular matrix nanocomposite scaffolds for potential bone tissue engineering*, Ceramics International, 51 (2025) 60419-60433.
https://doi.org/10.1016/j.ceramint.2025.10.242

Figs. 7(a) and (b) show the SEM images of the SF/30DCECM scaffold after soaking in SBF for 21 days. The scaffold exhibits a smooth surface with no significant precipitation, demonstrating its weak bioactive behavior. In contrast, as shown in Figs. 7(c) and (d), the surface morphology of the SF/30DCECM/15SrMBNs scaffold changes notably after 7 days of immersion. As can be seen, the formation of irregularly shaped crystals with a granular texture is obvious. Furthermore, the higher magnification image (Fig. 7(d)) shows cauliflower-like precipitates, characteristic of apatite crystals. Based on Figs. 7(e) and (f), a more compact and larger apatite crystals are formed after 21 days of immersion, suggesting a progressive apatite deposition process

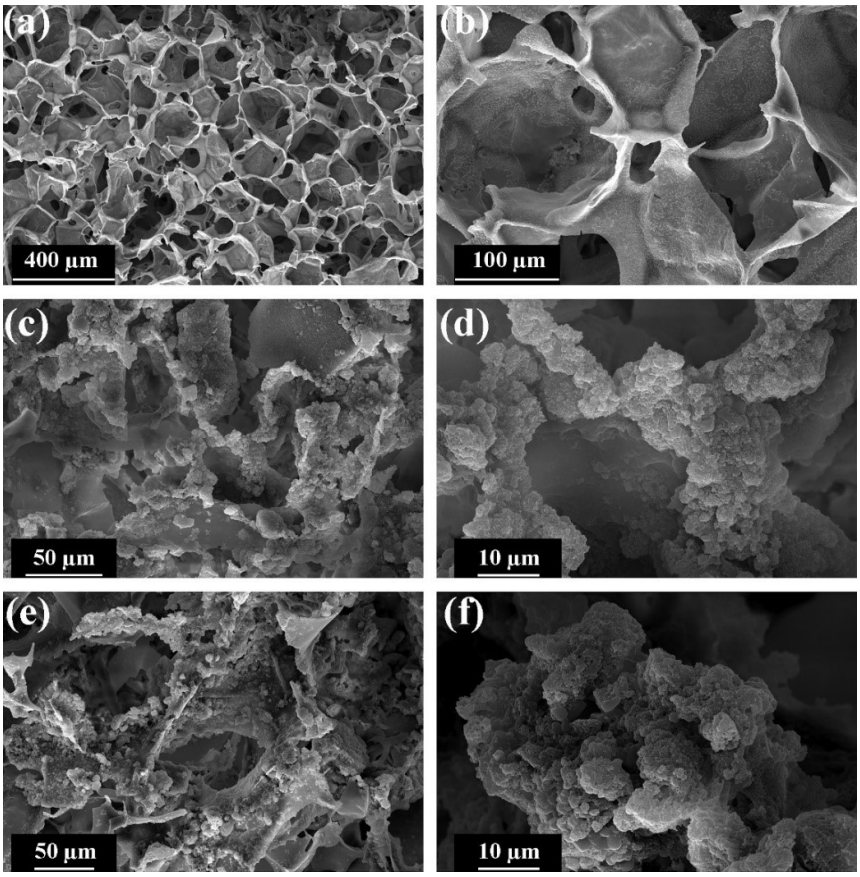

**This is the accepted manuscript (postprint) of the following article:**
F. Ghanbari, A.H. Taghvaei, E. Salahinejad, M. Pahlevani, Z. Khosrowpour, S.M.A. Haramshahi, M. Gholipourmalekabadi, *Strontium-doped mesoporous bioactive glass reinforced silk fibroin/decellularized extracellular matrix nanocomposite scaffolds for potential bone tissue engineering*, Ceramics International, 51 (2025) 60419-60433.
https://doi.org/10.1016/j.ceramint.2025.10.242

*Fig. 7. SEM images of the SF/30DCECM scaffold after immersion in SBF for 21 days (a, b), along with SEM images of the SF/30DCECM/15SrMBNs scaffold after 7 (c, d) and 21 (e, f) days of immersion in SBF.*

Based on Fig. 8(a), the SF/30DCECM scaffold exhibits a gradual weight loss up to 14 days of immersion in SBF, followed by a larger mass reduction with longer soaking time. This trend indicates that compared to the apatite formation, the SF/30DCECM scaffold degradation is dominant, especially after 14 days of soaking. In contrast, the SF/30DCECM/15SrMBNs scaffold shows a notably higher mass gain during the entire immersion period. This effect, which is consistent with the FESEM results demonstrates a noticeably greater content of precipitates. Moreover, the findings align with the data depicted in Fig. 6(b), illustrating that the inclusion of the SrMBNs into the SF/30DCECM scaffold leads to a more stable structure in terms of the degradation rate.

**This is the accepted manuscript (postprint) of the following article:**
F. Ghanbari, A.H. Taghvaei, E. Salahinejad, M. Pahlevani, Z. Khosrowpour, S.M.A. Haramshahi, M. Gholipourmalekabadi, *Strontium-doped mesoporous bioactive glass reinforced silk fibroin/decellularized extracellular matrix nanocomposite scaffolds for potential bone tissue engineering*, Ceramics International, 51 (2025) 60419-60433.
https://doi.org/10.1016/j.ceramint.2025.10.242

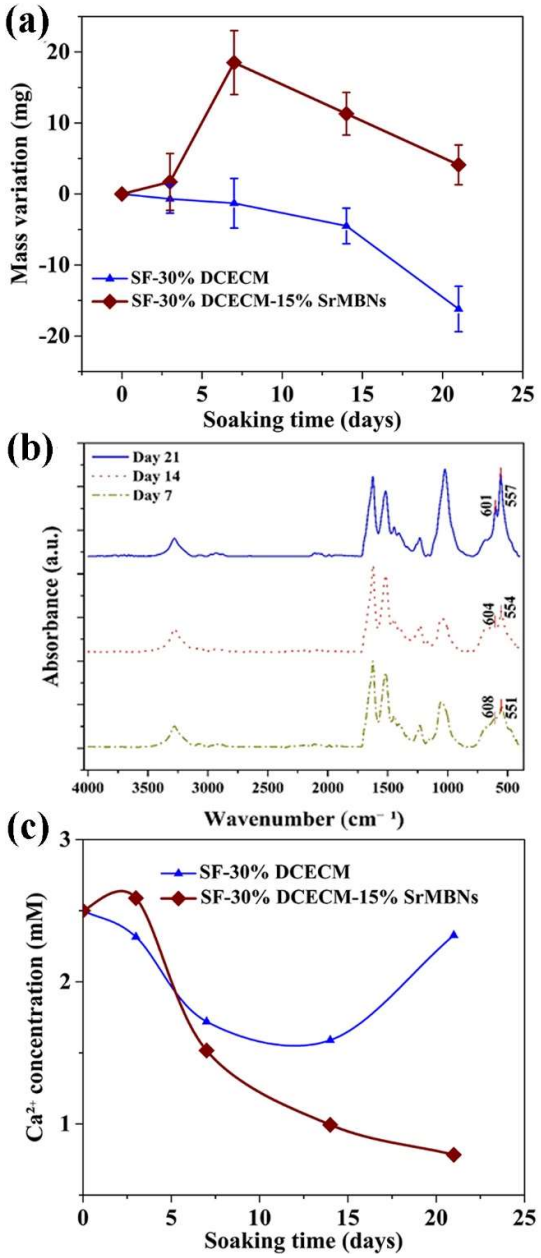


*Fig. 8. Mass variations of the SF/30DCECM and SF/30DCECM/15SrMBNs scaffolds upon immersion in SBF (a), FTIR spectra of the SF/30DCECM/15 SrMBNs scaffold after immersion in SBF (h), and variation of $Ca^{2+}$ in SBF during immersion of the SF/30DCECM and SF/30DCECM/15SrMBNs scaffolds.*

**This is the accepted manuscript (postprint) of the following article:**
F. Ghanbari, A.H. Taghvaei, E. Salahinejad, M. Pahlevani, Z. Khosrowpour, S.M.A. Haramshahi, M. Gholipourmalekabadi, *Strontium-doped mesoporous bioactive glass reinforced silk fibroin/decellularized extracellular matrix nanocomposite scaffolds for potential bone tissue engineering*, Ceramics International, 51 (2025) 60419-60433.
https://doi.org/10.1016/j.ceramint.2025.10.242

The EDS analysis on the SF/30DCECM/15SrMBNs scaffold after immersion in SBF (not shown) revealed the presence of Ca and P elements, with the ratios of 1.63 and 1.66 after soaking in SBF for 7 and 21 days, respectively. These ratios are close to the stoichiometric ratio for the hydroxyapatite crystals (1.67), proving their precipitation after immersion in SBF. Additionally, the Ca/P ratio of the scaffold remained relatively stable over time, demonstrating a consistent apatite formation and composition. The compositional changes on the surface of the SF/30DCECM/15SrMBNs scaffold and the formation of apatite crystals after soaking in SBF were further investigated by the ATR-FTIR analysis. Based on Fig. 8(b), the spectra indicate two distinct peaks around 600 and 560 $cm^{-1}$, corresponding to the vibration of the phosphate group ($PO_4^{3-}$) in the hydroxyapatite structure [45]. The intensity of these peaks increases over the soaking time, indicating a rise in the $PO_4^{3-}$ content and consequently an increase in the level of the apatite phase formed or its crystallinity on the surface of the scaffold.

The ion exchange phenomenon between SBF and the scaffold surface is an important factor in determining the degradation profile as well as the bioactivity of scaffolds [46]. The release of active ions, such as $Ca^{2+}$, $Si^{4+}$, and $Sr^{2+}$ from the SrMBNs plays a pivotal role in the formation of apatite, stimulating cell proliferation and inducing bone formation *in-vivo* [47-50]. The concentration of such ions depends on the balance between the release rate of ions from the scaffold and the formation rate of calcium phosphate-type crystals like hydroxyapatite. Fig. 8(c) shows the time-dependent evolution of the $Ca^{2+}$ concentration in SBF for the SF/30DCECM and SF/30DCECM/15SrMBNs scaffolds. The scaffolds incorporating the SrMBNs display an initial increase in the $Ca^{2+}$concentration after 2 days of soaking, followed by a relatively sharp decrease with extended immersion time up to 21 days. In

**This is the accepted manuscript (postprint) of the following article:**
F. Ghanbari, A.H. Taghvaei, E. Salahinejad, M. Pahlevani, Z. Khosrowpour, S.M.A. Haramshahi, M. Gholipourmalekabadi, *Strontium-doped mesoporous bioactive glass reinforced silk fibroin/decellularized extracellular matrix nanocomposite scaffolds for potential bone tissue engineering*, Ceramics International, 51 (2025) 60419-60433.
https://doi.org/10.1016/j.ceramint.2025.10.242

contrast, the SF/30DCECM scaffolds exhibit a gradual decline of $Ca^{2+}$ ions in SBF up to 14 days, and then an increase between 14 and 21 days. A significant depletion of $Ca^{2+}$ in SBF suggests its consumption and formation of a noticeable apatite phase content, as confirmed above. Compared to the SF/30DCECM/15SrMBNs sample, a higher $Ca^{2+}$ concentration in SBF for the SF/30DCECM scaffolds implies the less precipitation of calcium phosphate-type phases or even their dissolution. This results in an increase in the $Ca^{2+}$ content beyond 14 days, indicating a lower bioactivity of the latter sample.

### 3-7- Cell metabolic activity

The metabolic activity of rBMSCs cultured on the scaffolds was explored by the MTT assay after 3, 5, and 7 days (Fig. 9(a-c)). The scaffold groups show mean cell viabilities ranging from 76.7 to 98.9% on day 3 (Fig. 8(a)), 85.1 to 95.6% on day 5 (Fig. 9(b)), and 78.2 to 99.8% on day 7 (Fig. 9(c)), with respect to the control (scaffold-free wells). According to the ISO 10993-5 standard [51], scaffolds are considered cytotoxic if they reduce cell viability by more than 30%. Accordingly, the results confirm that all of the scaffolds exhibit acceptable cytocompatibility. Specifically, the SF/30DCECM and SF/30DCECM/15SrMBNs scaffolds demonstrated desired biocompatibility, with mean cell viabilities of 96.8, 93, and 92.75 for the former and 90, 93.1, and 91.5% for the latter on days 3, 5, and 7, respectively.

**This is the accepted manuscript (postprint) of the following article:**
F. Ghanbari, A.H. Taghvaei, E. Salahinejad, M. Pahlevani, Z. Khosrowpour, S.M.A. Haramshahi, M. Gholipourmalekabadi, *Strontium-doped mesoporous bioactive glass reinforced silk fibroin/decellularized extracellular matrix nanocomposite scaffolds for potential bone tissue engineering*, Ceramics International, 51 (2025) 60419-60433.
https://doi.org/10.1016/j.ceramint.2025.10.242

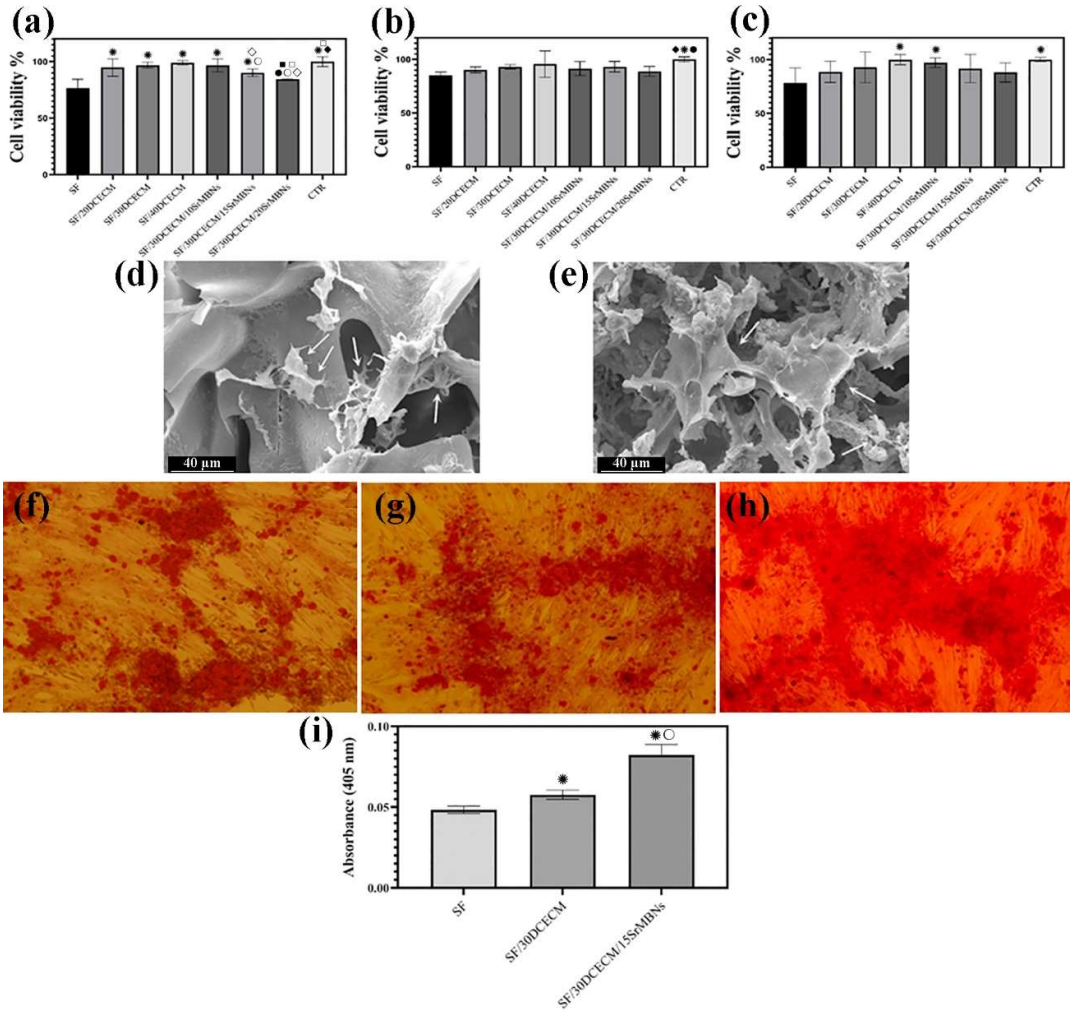


*Fig. 9. MTT cell viability results on the different scaffolds on days 3 (a), 5 (b), and 7 (c), cell attachment on the SF/30DCECM (d) and SF/DCECM/15SrMBNs (e) scaffolds on day 2, Alizarin red staining images of the SF (f), SF/30DCECM (g), and SF/30DCECM/15SrMBNs (h) scaffolds after 14 days of incubation with rBMSCs in the osteogenic medium, and quantification of Alizarin red staining with each group (i) (*, ●, ❍, ◇, ■, □, and ◆ denote significant differences relative to the SF, SF/20DCECM, SF/30DCECM, SF/40DCECM, SF/30DCECM/10 SrMBNs, SF/30DCECM/15 SrMBNs, and SF/30DCECM/20 SrMBNs in each chart, respectively, with $p < 0.05$).*

**This is the accepted manuscript (postprint) of the following article:**
F. Ghanbari, A.H. Taghvaei, E. Salahinejad, M. Pahlevani, Z. Khosrowpour, S.M.A. Haramshahi, M. Gholipourmalekabadi, *Strontium-doped mesoporous bioactive glass reinforced silk fibroin/decellularized extracellular matrix nanocomposite scaffolds for potential bone tissue engineering*, Ceramics International, 51 (2025) 60419-60433.
https://doi.org/10.1016/j.ceramint.2025.10.242

The SF scaffold exhibited the lowest cell viability on day 3. In contrast, the addition of DCECM notably enhanced cell viability and proliferation, regardless of its concentration. This effect is attributed to the presence and bioactive roles of ECM proteins like laminin, collagen, and fibronectin, which act as excellent cell adhesion motifs and provide a natural and favorable microenvironment conducive for cell growth [52]. Furthermore, this improved cell viability could result from the structural evolution from the lamellar to the 3D interconnected porous one (Fig. 2), as well as the increased swelling ratio (Fig. 6). Based on Fig. 9(a), the incorporation of 10% SrMBNs did not significantly change the cell metabolic activity on day 3. In contrast, the addition of 15 % SrMBNs slightly lowers the cell viability compared to the scaffolds containing 30 and 40 % DCECM, while it still exhibits a higher cell proliferation rate than the SF scaffold. The further addition of the nanoparticles to 20% reduced cell growth to a level comparable to the SF scaffold. This effect could be attributed to the suppressed porosity, pore size, and swelling ratio of the scaffolds or the excessive release of ions from SrMBNs [53, 54]. Cell viability became comparable across all the scaffold groups on 5 days of culture (Fig. 9b). However, on 7 days, an increase in the viability was observed for the SF/40DCECM and SF/30DCECM/10SrMBNs scaffolds relative to the pure SF scaffold. However, the viability of these two groups was not statistically different from that of the other samples.

### 3-8- Cell adhesion

Cell adhesion is the process by which cells attach to a surface substrate, which is essential for tissue formation and function. Cell adhesion can be influenced by various factors, such as the surface chemistry, topography, porosity, and stiffness of scaffolds, as well as the cell type,

**This is the accepted manuscript (postprint) of the following article:**
F. Ghanbari, A.H. Taghvaei, E. Salahinejad, M. Pahlevani, Z. Khosrowpour, S.M.A. Haramshahi, M. Gholipourmalekabadi, *Strontium-doped mesoporous bioactive glass reinforced silk fibroin/decellularized extracellular matrix nanocomposite scaffolds for potential bone tissue engineering*, Ceramics International, 51 (2025) 60419-60433.
https://doi.org/10.1016/j.ceramint.2025.10.242

density, and culture conditions [55, 56]. Fig. 9(d) illustrates the microscopic image of the SF/30DCECM scaffold cultured with rBMSCs for 48 h. As shown, the cells have spread out and attached well to the scaffold surface and interior of pores, exhibiting extended pseudopodia, indicative of active attachment to the scaffold. These pseudopodia are dynamic cellular extensions that facilitate cell-scaffold interactions [57]. The SF/30DCECM/15SrMBNs scaffold (Fig. 9(e)), following 48 h of incubation, demonstrates an irregular interconnected porous architecture, characterized by a rough surface texture with numerous protrusions and indentations. This intricate topography is likely to enhance cellular adhesion and interaction. As illustrated in the figure, the cells exhibit interconnectivity and adherence to the scaffold surface. However, they display an irregular morphology with a reduced spreading and a lower pseudopodia formation compared to the SF/30DCECM scaffold. This result aligns with a slightly lower cell proliferation observed on the SF/30DCECM/15SrMBNs scaffold compared to the SF/30DCECM scaffold, particularly after incubation for 3 days. Despite the increased in the surface roughness for the SrMBN-containing scaffold, it seems that the decrease in the ECM fraction and the corresponding cell adhesion motifs play a more dominant role in the cell attachment.

### 3-9- Osteogenic potential

The Alizarin red staining (ARS) technique is commonly used to detect calcium deposits during osteogenic differentiation and the subsequent mineralization of ECM. The ARS images and corresponding absorbance data for the SF, SF/30DCECM, and SF/30DCECM/15SrMBNs scaffolds after 14 days of incubation are shown in Fig. 9 (f-i). The bright red patches observed

**This is the accepted manuscript (postprint) of the following article:**
F. Ghanbari, A.H. Taghvaei, E. Salahinejad, M. Pahlevani, Z. Khosrowpour, S.M.A. Haramshahi, M. Gholipourmalekabadi, *Strontium-doped mesoporous bioactive glass reinforced silk fibroin/decellularized extracellular matrix nanocomposite scaffolds for potential bone tissue engineering*, Ceramics International, 51 (2025) 60419-60433.
https://doi.org/10.1016/j.ceramint.2025.10.242

in the SF scaffold image represent areas where $Ca^{2+}$ has bound to Alizarin molecules. The presence of calcium deposits suggests that the SF scaffold might have some inherent potential for mineralization. However, the sparse distribution of these red patches indicates that the SF alone may not be a highly conducive platform for robust mineralization and subsequent bone regeneration. In contrast, the addition of DCECM contributes to enhanced mineralization. This result demonstrates that the DCECM scaffolds are more conducive to mineralization than pure SF. The osteogenic capacity of placenta-derived DCECM is attributed to its rich biological composition containing collagen and glycosaminoglycan, providing an excellent structural and biomechanical foundation for bone tissue engineering. Additionally, the existence of cytokines and growth factors such as VEGF and BMP could play a pivotal role in osteogenic differentiation and promoting bone formation *in-vivo* [14, 58]. Furthermore, as shown before, the incorporation of DCECM modify the microstructure, physiochemical, and biomechanical properties of the scaffolds, contributing to the improved cell interaction and subsequent osteogenic differentiation.

The ARS results indicate that incorporating the SrMBNs into the SF/DCECM scaffold significantly enhances the osteogenic differentiation of rBMSCs. Based on the SEM results (Fig. 2), a homogeneous distribution of the SrMBNs within the SF/DCECM matrix not only provides a bone-like biomimetic microenvironment for cell growth and differentiation but also increases the surface area of the scaffolds for enhanced ion release [59]. Our previous results indicated that the SrMBNs could act as a platform for a sustain delivery of osteogenic $Sr^{2+}$ species [20]. Therefore, the release of osteoinductive ions from bioactive glass along with the inherent osteogenic activity of DCECM could synergistically promote the differentiation of MSCs. Furthermore, another factor contributing to the improved bone-like mineralization

**This is the accepted manuscript (postprint) of the following article:**
F. Ghanbari, A.H. Taghvaei, E. Salahinejad, M. Pahlevani, Z. Khosrowpour, S.M.A. Haramshahi, M. Gholipourmalekabadi, *Strontium-doped mesoporous bioactive glass reinforced silk fibroin/decellularized extracellular matrix nanocomposite scaffolds for potential bone tissue engineering*, Ceramics International, 51 (2025) 60419-60433.
https://doi.org/10.1016/j.ceramint.2025.10.242

ability by the SF/30DCECM/15SrMBNs scaffold is its higher bioactivity and formation of apatite crystals on its surface, offering an excellent osteoconductive and osteoinductive potential [60]. From a biomechanical point of view, it was shown that the addition of DCECM and the optimum content of the SrMBNs (15%) into SF could notably increase the stiffness of the scaffolds. (Fig. 5). Enhancing the stiffness of scaffolds is beneficial for better cell infiltration and proliferation, as well as for bone repair application [59]. It has been also demonstrated that a greater scaffold stiffness can upregulate the differentiation of MSCs toward the osteogenic lineage [59, 61]. Based on the mentioned data, the SF/30DCECM/15SrMBNs sample emerge as a highly effective composite scaffolds with the optimal physiochemical and mechanical properties, making it a promising candidate for bone tissue engineering.

## 4- Conclusion

Hierarchically-structured 3D porous SF/DCECM/SrMBNs scaffolds were successfully prepared via lyophilization; and their microstructure, physiochemical, mechanical, and bioperformance were systematically investigated. It was shown that the incorporation of 30% DCECM to SF drastically not only changed its architecture from lamellar to a highly porous structure but also significantly enhanced its elastic modulus, compressive strength, swelling ratio, and MSCs proliferation. While introducing 15 % SrMBNs to SF/DCECM decreased its compressive strength, it increased its elastic modulus and enhanced *in-vitro* apatite formation, without adversely affecting MSCs viability over extended culture periods. The ARS results represented that the presence of DCECM and SrMBNs can notably level up the osteogenic potential and mineralization of MSCs seeded on the SF/DCECM/SrMBNs scaffolds compared

**This is the accepted manuscript (postprint) of the following article:**
F. Ghanbari, A.H. Taghvaei, E. Salahinejad, M. Pahlevani, Z. Khosrowpour, S.M.A. Haramshahi, M. Gholipourmalekabadi, *Strontium-doped mesoporous bioactive glass reinforced silk fibroin/decellularized extracellular matrix nanocomposite scaffolds for potential bone tissue engineering*, Ceramics International, 51 (2025) 60419-60433.
https://doi.org/10.1016/j.ceramint.2025.10.242

to SF. Our results demonstrated that the SF/30DCECM/15SrMBNs scaffolds could be considered a promising platform for bone tissue-engineering applications due to their excellent biocompatibility and osteoinductivity.

## Acknowledgment

This study was financially supported by the Iran National Science Foundation (Grant No. 4030636). The authors also acknowledge the use of DeepSeek during the preparation of this paper to improve readability and language. After using this tool, the authors reviewed and edited the content as needed and take full responsibility for the content of the published article.

## Conflict of interest

The authors declare that they have no conflicts of interests.

## References

[1] N. Su, J. Yang, Y. Xie, X. Du, H. Chen, H. Zhou, L. Chen, Bone function, dysfunction and its role in diseases including critical illness, Int. J. Biol. Sci. 15(4) (2019) 776–787. https://doi.org/10.7150/ijbs.27063.

[2] B. Clarke, Normal bone anatomy and physiology, Clin. J. Am. Soc. Nephrol. 3(3) (2008) S131-S139. https://doi.org/10.2215/CJN.04151206

[3] T.A. St John, A.R. Vaccaro, A.P. Sah, M. Schaefer, S.C. Berta, T. Albert, A. Hilibrand, Physical and monetary costs associated with autogenous bone graft harvesting, Am. J. Orthop. 32(1) (2003) 18-23.

[4] A.R. Amini, C.T. Laurencin, S.P. Nukavarapu, Bone tissue engineering: recent advances and challenges, Crit. Rev. Biomed. Eng. 40(5) (2012) 363-408. https://doi.org/10.1615/CritRevBiomedEng.v40.i5.10.

[5] G.L. Koons, M. Diba, A.G. Mikos, Materials design for bone-tissue engineering, Nat. Rev. Mater. 5(8) (2020) 584-603. https://doi.org/10.1038/s41578-020-0204-2.

[6] B. Kundu, R. Rajkhowa, S.C. Kundu, X. Wang, Silk fibroin biomaterials for tissue regenerations, Adv. Drug Deliv. Rev. 65 (2013) 457-470. https://doi.org/10.1016/j.addr.2012.09.043.

**This is the accepted manuscript (postprint) of the following article:**
F. Ghanbari, A.H. Taghvaei, E. Salahinejad, M. Pahlevani, Z. Khosrowpour, S.M.A. Haramshahi, M. Gholipourmalekabadi, *Strontium-doped mesoporous bioactive glass reinforced silk fibroin/decellularized extracellular matrix nanocomposite scaffolds for potential bone tissue engineering*, Ceramics International, 51 (2025) 60419-60433.
https://doi.org/10.1016/j.ceramint.2025.10.242

[7] S. Zhu, Q. Zhang, X. Xu, Z. Liu, G. Cheng, D. Long, L. Cheng, F. Dai, Recent advances in silk fibroin-based composites for bone repair pplications: a review, Polymers 17(6) (2025) 772. https://doi.org/10.3390/polym17060772.

[8] Z. Mao, X. Bi, C. Yu, L. Chen, J. Shen, Y. Huang, Z. Wu, H. Qi, J. Guan, X. Shu, Mechanically robust and personalized silk fibroin-magnesium composite scaffolds with water-responsive shape-memory for irregular bone regeneration, Nature Communications 15(1) (2024) 4160. https://doi.org/10.1038/s41467-024-48417-8.

[9] X. Bi, Z. Mao, Y. Zhang, Z. Ren, K. Yang, C. Yu, L. Chen, R. Zheng, J. Guan, Z. Liu, Endogenous dual-responsive and self-adaptive silk fibroin-based scaffold with enhancement of immunomodulation for skull regeneration, Biomaterials 320 (2025) 123261. https://doi.org/10.1016/j.biomaterials.2025.123261.

[10] M. Farokhi, F. Mottaghitalab, S. Samani, M.A. Shokrgozar, S.C. Kundu, R.L. Reis, Y. Fatahi, D.L. Kaplan, Silk fibroin/hydroxyapatite composites for bone tissue engineering, Biotechnol. Adv. 36(1) (2018) 68-91. https://doi.org/10.1016/j.biotechadv.2017.10.001.

[11] H. Wu, K. Lin, C. Zhao, X. Wang, Silk fibroin scaffolds: A promising candidate for bone regeneration, Front. Bioeng. Biotechnol. 10 (2022) 1054379. https://doi.org/10.3389/fbioe.2022.1054379.

[12] Y.S. Kim, M. Majid, A.J. Melchiorri, A.G. Mikos, Applications of decellularized extracellular matrix in bone and cartilage tissue engineering, Bioeng. Transl. Med. 4(1) (2019) 83-95. https://doi.org/10.1002/btm2.10110.

[13] D.E. Heath, A review of decellularized extracellular matrix biomaterials for regenerative engineering applications, Regen. Eng. Transl. Med. 5 (2019) 155-166. https://doi.org/10.1007/s40883-018-0080-0.

[14] A.P. Rameshbabu, K. Bankoti, S. Datta, E. Subramani, A. Apoorva, P. Ghosh, S. Jana, P. Manchikanti, S. Roy, K. Chaudhury, Bioinspired 3D porous human placental derived extracellular matrix/silk fibroin sponges for accelerated bone regeneration, Mater. Sci. Eng. C 113 (2020) 110990. https://doi.org/10.1016/j.msec.2020.110990.

[15] V. Rukosuev, Immunofluorescent localization of collagen types I, III, IV, V, fibronectin, laminin, entactin, and heparan sulphate proteoglycan in human immature placenta, Experientia 48 (1992) 285-287. https://doi.org/10.1007/BF01930477.

[16] B. Labat, A. Chamson, J. Frey, Effects of γ-alumina and hydroxyapatite coatings on the growth and metabolism of human osteoblasts, J. Biomed. Mater. Res. 29(11) (1995) 1397-1401. https://doi.org/10.1002/jbm.820291111.

[17] M. Vallet-Regi, A.J. Salinas, Mesoporous bioactive glasses for regenerative medicine, Mater. Today Bio 11 (2021) 100121. https://doi.org/10.1016/j.mtbio.2021.100121.

[18] D. Lin, K. Yang, W. Tang, Y. Liu, Y. Yuan, C. Liu, A poly (glycerol sebacate)-coated mesoporous bioactive glass scaffold with adjustable mechanical strength, degradation rate, controlled-release and cell behavior for bone tissue engineering, Colloids Surf. B Biointerfaces 131 (2015) 1-11. https://doi.org/10.1016/j.colsurfb.2015.04.031.

[19] T. Sun, M. Liu, S. Yao, Y. Ji, Z. Xiong, K. Tang, K. Chen, H. Yang, X. Guo, Biomimetic composite scaffold containing small intestinal submucosa and mesoporous bioactive glass exhibits high osteogenic and angiogenic capacity, Tissue Eng. Part A 24(13-14) (2018) 1044-1056. https://doi.org/10.1089/ten.TEA.2017.0398.

[20] A.H. Taghvaei, F. Danaeifar, C. Gammer, J. Eckert, S. Khosravimelal, M. Gholipourmalekabadi, Synthesis and characterization of novel mesoporous strontium-modified bioactive glass nanospheres for bone tissue engineering applications, Microporous Mesoporous Mater. 294 (2020) 109889. https://doi.org/10.1016/j.micromeso.2019.109889.

[21] C. Wu, Y. Zhang, Y. Zhou, W. Fan, Y. Xiao, A comparative study of mesoporous glass/silk and non-mesoporous glass/silk scaffolds: physiochemistry and in vivo osteogenesis, Acta Biomater. 7 (2011) 2229-2236. https://doi.org/10.1016/j.actbio.2010.12.019.

[22] A. Chandrasekaran, G. Novajra, I. Carmagnola, P. Gentile, S. Fiorilli, M. Miola, M. Boregowda, A. Dakshanamoorthy, G. Ciardelli, C. Vitale-Brovarone, Physico-chemical and biological studies on three-dimensional porous silk/spray-dried mesoporous bioactive glass scaffolds, Ceram. Int. 42(12) (2016) 13761-13772. https://doi.org/10.1016/j.ceramint.2016.05.176.

[23] S. Sangkert, S. Kamonmattayakul, W.L. Chai, J. Meesane, A biofunctional-modified silk fibroin scaffold with mimic reconstructed extracellular matrix of decellularized pulp/collagen/fibronectin for bone tissue engineering in alveolar bone resorption, Mater. Lett. 166 (2016) 30-34. https://doi.org/10.1016/j.matlet.2015.12.032.

[24] D.N. Rockwood, R.C. Preda, T. Yücel, X. Wang, M.L. Lovett, D.L. Kaplan, Materials fabrication from Bombyx mori silk fibroin, Nat. Protoc. 6(10) (2011) 1612-1631. https://doi.org/10.1038/nprot.2011.379.

**This is the accepted manuscript (postprint) of the following article:**
F. Ghanbari, A.H. Taghvaei, E. Salahinejad, M. Pahlevani, Z. Khosrowpour, S.M.A. Haramshahi, M. Gholipourmalekabadi, *Strontium-doped mesoporous bioactive glass reinforced silk fibroin/decellularized extracellular matrix nanocomposite scaffolds for potential bone tissue engineering*, Ceramics International, 51 (2025) 60419-60433.
https://doi.org/10.1016/j.ceramint.2025.10.242

[25] D.O. Freytes, J. Martin, S.S. Velankar, A.S. Lee, S.F. Badylak, Preparation and rheological characterization of a gel form of the porcine urinary bladder matrix, Biomaterials 29(11) (2008) 1630-1637. https://doi.org/10.1016/j.biomaterials.2007.12.014

[26] Y. Wang, X. Chatzistavrou, D. Faulk, S. Badylak, L. Zheng, S. Papagerakis, L. Ge, H. Liu, P. Papagerakis, Biological and bactericidal properties of Ag-doped bioactive glass in a natural extracellular matrix hydrogel with potential application in dentistry, Eur. Cell. Mater. 29 (2015) 342-355. https://doi.org/10.22203/ecm.v029a26.

[27] M.M. Islam, D.B. AbuSamra, A. Chivu, P. Argüeso, C.H. Dohlman, H.K. Patra, J. Chodosh, M. González-Andrades, Optimization of collagen chemical crosslinking to restore biocompatibility of tissue-engineered scaffolds, Pharmaceutics 13(6) (2021) 832. https://doi.org/10.3390/pharmaceutics13060832.

[28] H.J. Kim, M.K. Kim, K.H. Lee, S.K. Nho, M.S. Han, I.C. Um, Effect of degumming methods on structural characteristics and properties of regenerated silk, Int. J. Biol. Macromol. 104 (2017) 294-302. https://doi.org/10.1016/j.ijbiomac.2017.06.019.

[29] A.P. Rameshbabu, K. Bankoti, S. Datta, E. Subramani, A. Apoorva, P. Ghosh, P.P. Maity, P. Manchikanti, K. Chaudhury, S. Dhara, Silk sponges ornamented with a placenta-derived extracellular matrix augment full-thickness cutaneous wound healing by stimulating neovascularization and cellular migration, ACS Appl. Mater. Interfaces 10 (2018) 16977-16991. https://doi.org/10.1021/acsami.7b19007.

[30] E. Mazzoni, C. Mazziotta, M.R. Iaquinta, C. Lanzillotti, F. Fortini, A. D'Agostino, L. Trevisiol, R. Nocini, G. Barbanti-Brodano, A. Mescola, Enhanced osteogenic differentiation of human bone marrow-derived mesenchymal stem cells by a hybrid hydroxylapatite/collagen scaffold, Front. Cell Dev. Biol. 8 (2021) 610570. https://doi.org/10.3389/fcell.2020.610570.

[31] V. Karageorgiou, D. Kaplan, Porosity of 3D biomaterial scaffolds and osteogenesis, Biomaterials 26(27) (2005) 5474-5491. https://doi.org/10.1016/j.biomaterials.2005.02.002.

[32] Q. Lv, Q. Feng, K. Hu, F. Cui, Three-dimensional fibroin/collagen scaffolds derived from aqueous solution and the use for HepG2 culture, Polymer 46(26) (2005) 12662-12669. https://doi.org/10.1016/j.polymer.2005.10.137.

[33] Q. Lu, X. Zhang, X. Hu, D.L. Kaplan, Green process to prepare silk fibroin/gelatin biomaterial scaffolds, Macromol. Biosci. 10(3) (2010) 289-298. https://doi.org/10.1002/mabi.200900258.

[34] M.M. Nava, L. Draghi, C. Giordano, R. Pietrabissa, The effect of scaffold pore size in cartilage tissue engineering, J. Appl. Biomater. Funct. Mater. 14(3) (2016) e223-e229. https://doi.org/10.5301/jabfm.5000302.

[35] Y. Ji, X. Yang, Z. Ji, L. Zhu, N. Ma, D. Chen, X. Jia, J. Tang, Y. Cao, DFT-calculated IR spectrum amide I, II, and III band contributions of N-methylacetamide fine components, ACS Omega 5 (2020) 8572-8578. https://doi.org/10.1021/acsomega.9b04421.

[36] S. Zarzhitsky, H. Edri, Z. Azoulay, I. Cohen, Y. Ventura, A. Gitelman, H. Rapaport, The effect of pH and calcium ions on the stability of amphiphilic and anionic β-sheet peptide hydrogels, Biopolymers 100(6) (2013) 760-772. https://doi.org/10.1002/bip.22282.

[37] N. Roamcharern, S.A. Matthew, D.J. Brady, J.A. Parkinson, Z. Rattray, F.P. Seib, Biomimetic silk nanoparticle manufacture: calcium ion-mediated assembly, ACS Biomater. Sci. Eng. 11(3) (2025) 1847-1856. https://doi.org/10.1021/acsbiomaterials.4c02175.

[38] G. Carissimi, C.M. Baronio, M.G. Montalbán, G. Víllora, A. Barth, On the secondary structure of silk fibroin nanoparticles obtained using ionic liquids: an infrared spectroscopy study, Polymers 12(6) (2020) 1294. https://doi.org/10.3390/polym12061294.

[39] E.-L. Karjalainen, H.K. Ravi, A. Barth, Simulation of the amide I absorption of stacked β-sheets, J. Phys. Chem. B 115(4) (2011) 749-757. https://doi.org/10.1021/jp109918c.

[40] Y.N. Chirgadze, B. Shestopalov, S.Y. Venyaminov, Intensities and other spectral parameters of infrared amide bands of polypeptides in the β-and random forms, Biopolymers 12(6) (1973) 1337-1351. https://doi.org/10.1002/bip.1973.360120610.

[41] M.R. Bidgoli, I. Alemzadeh, E. Tamjid, M. Khafaji, M. Vossoughi, Fabrication of hierarchically porous silk fibroin-bioactive glass composite scaffold via indirect 3D printing: Effect of particle size on physico-mechanical properties and in vitro cellular behavior, Mater. Sci. Eng. C 103 (2019) 109688. https://doi.org/10.1016/j.msec.2019.04.067.

[42] M. Peter, N. Binulal, S. Nair, N. Selvamurugan, H. Tamura, R. Jayakumar, Novel biodegradable chitosan–gelatin/nano-bioactive glass ceramic composite scaffolds for alveolar bone tissue engineering, Chem. Eng. J. 158(2) (2010) 353-361. https://doi.org/10.1016/j.cej.2010.02.003.

**This is the accepted manuscript (postprint) of the following article:**
F. Ghanbari, A.H. Taghvaei, E. Salahinejad, M. Pahlevani, Z. Khosrowpour, S.M.A. Haramshahi, M. Gholipourmalekabadi, *Strontium-doped mesoporous bioactive glass reinforced silk fibroin/decellularized extracellular matrix nanocomposite scaffolds for potential bone tissue engineering*, Ceramics International, 51 (2025) 60419-60433.
https://doi.org/10.1016/j.ceramint.2025.10.242

[43] S. Tajvar, A. Hadjizadeh, S.S. Samandari, Scaffold degradation in bone tissue engineering: an overview, Int. Biodeterior. Biodegrad. 180 (2023) 105599. https://doi.org/10.1016/j.ibiod.2023.105599.

[44] P. Pei, D. Wei, M. Zhu, X. Du, Y. Zhu, The effect of calcium sulfate incorporation on physiochemical and biological properties of 3D-printed mesoporous calcium silicate cement scaffolds, Microporous Mesoporous Mater. 241 (2017) 11-20. https://doi.org/10.1016/j.micromeso.2016.11.031.

[45] I. Rehman, W. Bonfield, Characterization of hydroxyapatite and carbonated apatite by photo acoustic FTIR spectroscopy, J. Mater. Sci. Mater. Med. 8(1) (1997) 1-4. https://doi.org/10.1023/a:1018570213546.

[46] F. Baino, S. Yamaguchi, The use of simulated body fluid (SBF) for assessing materials bioactivity in the context of tissue engineering: review and challenges, Biomimetics 5(4) (2020) 57. https://doi.org/10.3390/biomimetics5040057.

[47] C. Wu, Y. Ramaswamy, D. Kwik, H. Zreiqat, The effect of strontium incorporation into CaSiO3 ceramics on their physical and biological properties, Biomaterials 28(21) (2007) 3171-3181. https://doi.org/10.1016/j.biomaterials.2007.04.002.

[48] C. Wu, J. Chang, Degradation, bioactivity, and cytocompatibility of diopside, akermanite, and bredigite ceramics, J. Biomed. Mater. Res. B Appl. Biomater. 83(1) (2007) 153-160. https://doi.org/10.1002/jbm.b.30779.

[49] P. Mazón, N. Piedad, Porous scaffold prepared from α′ L-Dicalcium silicate doped with phosphorus for bone grafts, Ceram. Int. 44(1) (2018) 537-545. https://doi.org/10.1016/j.ceramint.2017.09.208.

[50] M. Gandolfi, G. Spagnuolo, F. Siboni, A. Procino, V. Rivieccio, G. Pelliccioni, C. Prati, S. Rengo, Calcium silicate/calcium phosphate biphasic cements for vital pulp therapy: chemical-physical properties and human pulp cells response, Clin. Oral Investig. 19(8) (2015) 2075-2089. https://doi.org/10.1007/s00784-015-1443-2.

[51] International Organization for Standardization. ISO 10993-5:2009, Biological evaluation of medical devices—Part 5: Tests for in vitro cytotoxicity, ISO, 2009, pp. 1-34.

[52] S. Yi, F. Ding, L. Gong, X. Gu, Extracellular matrix scaffolds for tissue engineering and regenerative medicine, Curr. Stem Cell Res. Ther. 12(3) (2017) 233-246. https://doi.org/10.2174/1574888X11666160905092513.

[53] L.L. Hench, Genetic design of bioactive glass, J. Eur. Ceram. Soc. 29(7) (2009) 1257-1265. https://doi.org/10.1016/j.jeurceramsoc.2008.08.002.

[54] A. Parvinnasab, S. Rostami, A. Namdar, E. Salahinejad, A.H. Taghvaei, S. Abdi, S. Rajabi, L. Tayebi, Balanced enhancement of antibacterial activity and biocompatibility in chitosan-vancomycin 3D-printed scaffolds through mesoporous bioactive glass addition, J. Drug Deliv. Sci. Technol. (2025) 106637. https://doi.org/10.1016/j.jddst.2025.106637.

[55] A.M. Ross, Z. Jiang, M. Bastmeyer, J. Lahann, Physical aspects of cell culture substrates: topography, roughness, and elasticity, Small 8(3) (2012) 336-355. https://doi.org/10.1002/smll.201100934.

[56] K. Anselme, L. Ploux, A. Ponche, Cell/material interfaces: influence of surface chemistry and surface topography on cell adhesion, J. Adhes. Sci. Technol. 24(5) (2010) 831-852. https://doi.org/10.1163/016942409X12598231568186.

[57] Y.A. Rovensky, Pseudopodia and Adhesion Structures, in: Adhes. Interact. Norm. Transf. Cells, Humana Press, 2011, pp. 37-56. https://doi.org/10.1007/978-1-61779-304-2_4.

[58] Z. Khosrowpour, S.M. Hashemi, S. Mohammadi-Yeganeh, S. Simorgh, B.S. Eftekhari, P. Brouki Milan, S.C. Kundu, M. Gholipourmalekabadi, Decellularized placental sponge: a platform for coculture of mesenchymal stem cells/macrophages to assess an M2 phenotype and osteogenic differentiation in vitro and in vivo, ACS Omega 9 (2024) 5298-5318. https://doi.org/10.1021/acsomega.3c06175.

[59] E.J. Ryan, A.J. Ryan, A. González-Vázquez, A. Philippart, F.E. Ciraldo, C. Hobbs, V. Nicolosi, A.R. Boccaccini, C.J. Kearney, F.J. O'Brien, Collagen scaffolds functionalised with copper-eluting bioactive glass reduce infection and enhance osteogenesis and angiogenesis both in vitro and in vivo, Biomaterials 197 (2019) 405-416. https://doi.org/10.1016/j.biomaterials.2019.01.031.

[60] L. Lin, K.L. Chow, Y. Leng, Study of hydroxyapatite osteoinductivity with an osteogenic differentiation of mesenchymal stem cells, J. Biomed. Mater. Res. A 89(2) (2009) 326-335. https://doi.org/10.1002/jbm.a.31994.

[61] R.G. Breuls, T.U. Jiya, T.H. Smit, Scaffold stiffness influences cell behavior: opportunities for skeletal tissue engineering, Open Orthop. J. 2 (2008) 103. https://doi.org/10.2174/1874325000802010103.